Master thesis 2006

Espen Flage-Larsen

April 9, 2006

Contents

1 The quantum dot

1.1 Artificial atom and how are they related to quantum dots

The quantum dot is a vague name, but it's often characterized as a conducting "island" with a size comparable to the Fermi wavelength. Usually this "island" is a residence for a number of electrons. The similarities between quantum dots and atoms are present, but there are significant differences. First of all the length scales in a quantum dots is different from any atom. A typical quantum dot have a length scale in the 100nm range, while atoms are smaller, ranging from about 0.05nm to 0.4nm. The confining forces are also different. In atoms, the attractive force is set up by the nucleus. But in quantum dots we typically have some external field which generates a background charge, thereby confining the particles. Since the length scale is different, the energy scale is also different. Typical values for a atom and a quantum dot is listed in Table 1.1.1 Despite the

	Quantum dot	Atom
Size	100nm	0.1nm
Energy spacing	0.1meV	1eV
Excitation energy	0,1meV	10eV
Magnetic field	10T	10000T

Table 1.1.1: Difference between a typical atom and quantum dot

difference, quantum dots are often called "artificial atoms". The difference lies in the scaling, but not the working. The quantum dots experience energy bands and excitation just like the atoms. They even show "magic numbers" seen in atoms, although with different values. By controlling the external potential we can determine the number of electrons in the quantum dot showing the analogy with the periodic table and shell filling.

Why is quantum dots so important to explore? The reason is two-folded. The first has to do with our need to manufacture smaller and smaller devices. As was mentioned at the very first of this section, the integrated circuits are reaching their maximum operation points due to size. For 15 years ago, quantum dots was not of any particular interest to people doing circuit layout and manufacturing. Today, this situation is far from the truth and research in this field is intense, judging by the number of published articles. Typical transistor operation is a switch that is turned on and of when a voltage is added. Transistors today are building bricks of all integrated electronics. The ultimate transistor would be one that turns on and of when one electron is added or removed, what we call SET (Single Electron Transistor) today. This is also a perfect quantum dot. Knowing its inner workings are essential in a manufacture process.

But in addition to the need of smaller transistors, the quantum dot as a artificial atom have opened a whole new area of research. One thing that makes quantum dots very special are the possibility to control their size, shape, dimension, energy bands and number of electrons. This is something we cannot do with regular atoms. So quantum dots turn out to be a very handy platform for

investigating many-body physics. One could also make several interacting quantum dots and form a lattice with shapes not found in nature. Even "artificial molecules" can also be made. This opens up a new world for basic research.

1.2 Structure, manufacture and operational principle

The manufacture process involved making quantum dots is complicated. You need high precision, material purity and a sophisticated controlling device. One of the first method for making quantum dots was developed by Reed et al. [17] during the mid 1980s. The common etching method today is more or less the same, just that the quality in the production is far better. The shape and operation principle is different from design to design, but all need to be produced on a small scale, typically 10-100nm to yield size quantization. Common semiconductor material is normally used. $GaAs$ (Gallium Arsenide) is preferred over Si (Silicon) due to its electrical properties. $GaAs$ have higher electron mobility, lower breakdown voltages and less noise. $GaAs$ can then be made smaller. However Silicon is easy available from quartz sand and are cheap. Silicon also bonds with oxides without problems and SiO_2 makes an excellent isolator. In addition, hole mobility is greater than $GaAs$. This gives Silicon the advantage when logical gates need to be produces, due to the potential higher speed of a Silicon p-channel transistor over $GaAs$. When you want to manufacture quantum dots mainly for measurements and research, size and error is more important than cost and speed. $GaAs$ can be combined with Aluminum to make a isolator. $AlAs$ (Aluminum Arsenide) is also a good insulator and both of these combine well with $GaAs$.

To make quantum dots, several methods and designs are available. Manufacturing is not the main topic in this thesis and we will just outline some of the techniques. The outline is the same for all methods. You start with a given dimension and reduce it to create a confinement of some sort, either physical or by some other means, for example electrical fields.

1.2.1 Size restriction using physical boundaries

To make a quantum dot which is physical restricted in one or two dimension we usually use etching. As we have mentioned before, this was the first technique developed and has become the most common since the middle of the 1980s. To prepare the sample for etching one uses lithography. A basic process for making several small transistors and connect them are illustrated in Figure 1.2.1. This process is an analogy to what's going on during the manufacture of quantum dots using lithography and etching. However, since we need far better precision electron or ion beam lithography is used instead of light. First you start with a Silicon or any other material of choice in a wafer form. The making of wafers are dependent on what characteristics you want in the end. Figure 1.2.2(a) show a typical sample of a quantum device. The bottom layer of $GaAs$ is doped to work as a reservoir. Then follows a barrier of $AlGaAs$ which act as a potential barrier to isolate the next $GaAs$ layer by tunneling. The top layer of Au works as a electrode. Because of the potential difference between $GaAs$ and $AlGaAs$ this wafer traps electrons in the middle $GaAs$ layer and we have a quantum dot. If we make the two barriers different in such way that electrons can tunnel over one of the barrier, but not the other we can control the electron flow on

and of the isolated layer in between. The wafer is layered with a mask on top. By using electron beam lithography, a pattern is made in the mask. We then expose the sample for a etching solution that only etch areas not protected by the mask. Finally we deposit ions to dope the material exposed, or we add a suitable metal. The metal can for example function as an electrode. In the end we're left with a smaller sized confinement as in Figure 1.2.2(b). When we apply potential difference between the electrode and the buffer, we can control the population of electrons inside the middle $GaAs$ layer. The form of these quantum dots can vary from design to design, but the principles are the same.

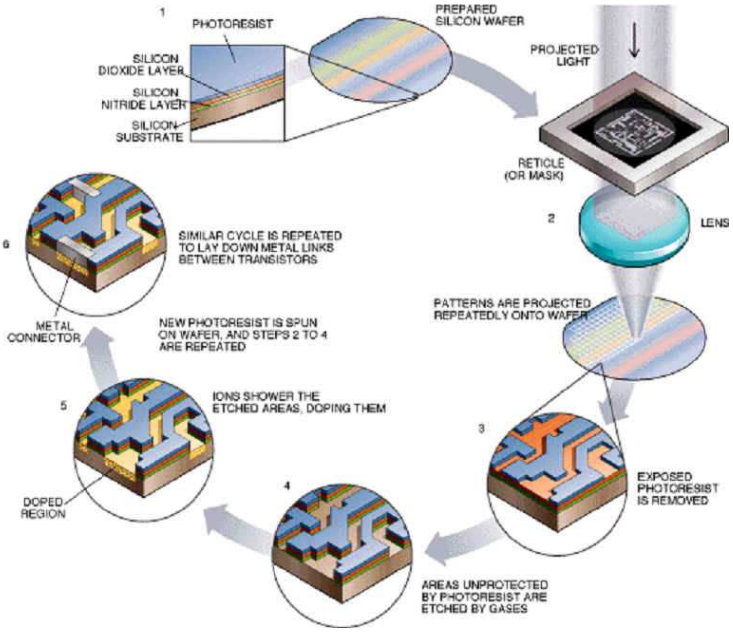

Figure 1.2.1: Light lithography used to create advanced integrated circuits

1.2.2 Size restriction using electrical fields

The etching technique is a physical process and if we need to change some variable in the produced dot, other than the potential difference between the buffer and the electrode, we need to manufacture another sample. This can be time consuming. We also introduce other deviations in data if we where to compare samples from two different production runs. The manufacture process cannot produce the exact same sample twice. Another method using lithography on a substrate to make conductors is more flexible. One example is shown in Figure 1.2.3. Here lithography is used to carve out the conductors on top of a $GaAlAs$ layer covered with a mask. We then deposit metal on top, usually gold. By applying potential difference between the finger gate and Q_1 and Q_2 we form what is called QPC (Quantum Point Contacts) which regulates the population of the isolated dot between the barriers by tunneling. We can then regulate the potential on the center gate to give geometric properties wanted in the dot. On each side of the QPCs we have drain and source. So, by using electrical fields

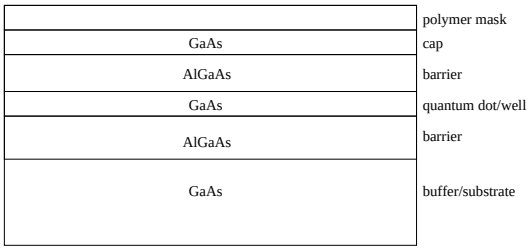

(a) Wafer

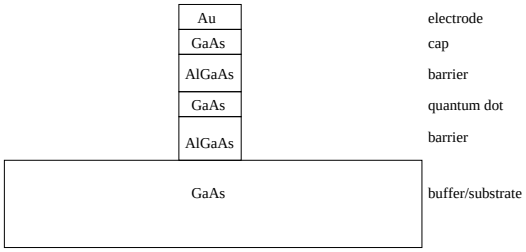

(b) End result

Figure 1.2.2: Layers in $GaAs$ quantum dot sample

we have greater flexibility. Another important feature is that we have no, or very little edge effects compared to the physical confinement.

There are several other methods developed, but the two explained here are the most useful. For the curious reader, what is called selective growth is outlined by Fukui et al. [6] and Lebens et al. [10]. Microcrystal semiconductors by Ekimov et al. [4]. Self-assembled dots are promising due to their small confinement size down to about 30nm. Experiments have been done by Marzin et al. [11] and Raymond et al. [16]

1.3 Charge quantization

In addition to size quantization we also have what is called charge quantization. In electromagnetism we have a well known device known as the capacitor. Two metal plates are spaced so they are isolated. Then a potential is applied over the plates. This cause a build up of charge at one plate and a reduction of equal charge on the other. In this way the capacitor stores energy. The displaced charge are electron gas and the charge buildup is more or less continuous with applied potential. It's not quantized. One defines Capacitance as the difference between the charges q and the potential V between the plates, $C = q/V$. The energy stored in a capacitor is defined as $E = q^2/2C$.

If we now make the distance between the plates small so it acts as a tunnel junction, the charge transfer between the plates is quantized. This mechanism is called Coulomb blockage. To outline the Coulomb blockage model, let us look at Figure 1.2.3. The island is isolated between two QPC, which work as tunneling barriers. We can now think of the island and the two QPCs as a quantized capacitor. This is a approximation since we've completely disregarded the Pauli exclusion principle, which also adds to the energy difference, but it is suppressed in comparison. The potential difference between the two gates is

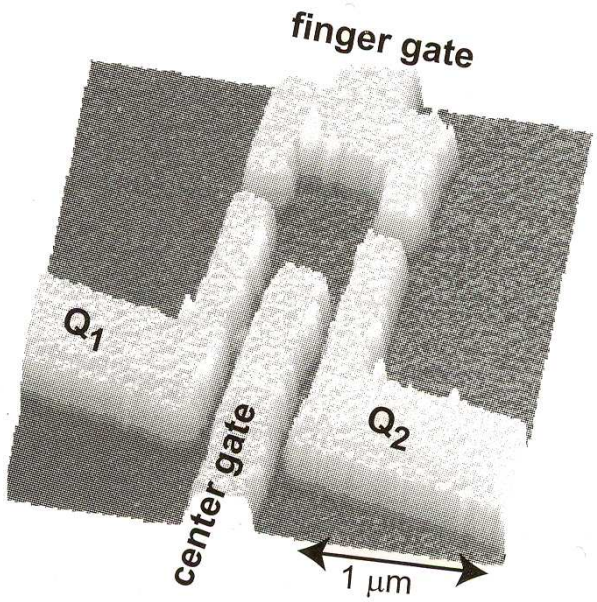

Figure 1.2.3: Typical quantum dot layout. From [8]

a bit more complex than in a regular capacitor, due to the presence of several gates. But let us call it V_g for simplicity. If we add a charge q to the island, the change in energy would be

$$\Delta E = qV_g + \frac{q^2}{2C} \tag{1.1}$$

The first term accounts for the work involved moving in the potential field, while the second is the energy of Coulomb repulsion of the island, the capacitor. The electron, either single or multiple is responsible for the charge transfer. For N electrons with charge $-e$ we have that $q = -Ne$. This give the energy difference as a function of the electron number n

$$\Delta E(n) = -NeV_g + N^2\frac{e^2}{2C} \tag{1.2}$$

The change in energy from $n+1$ electron to n electron is given as

$$\Delta E(n+1) - E(n) = -eV_g + (\frac{1}{2} + n)\frac{e^2}{C} \tag{1.3}$$

When the energy difference vanish, electrons can be transfered on and off the island. This happens when the gate potential is

$$V_g = \left(\frac{1}{2} + n\right)\frac{e}{C} \tag{1.4}$$

This give rise to a special property regarding current flow through the islands of quantum dots. A plot of conductance as a function of gate potential is shown in Figure 1.3.4. We see that Coulomb blockage occur between the peaks. However,

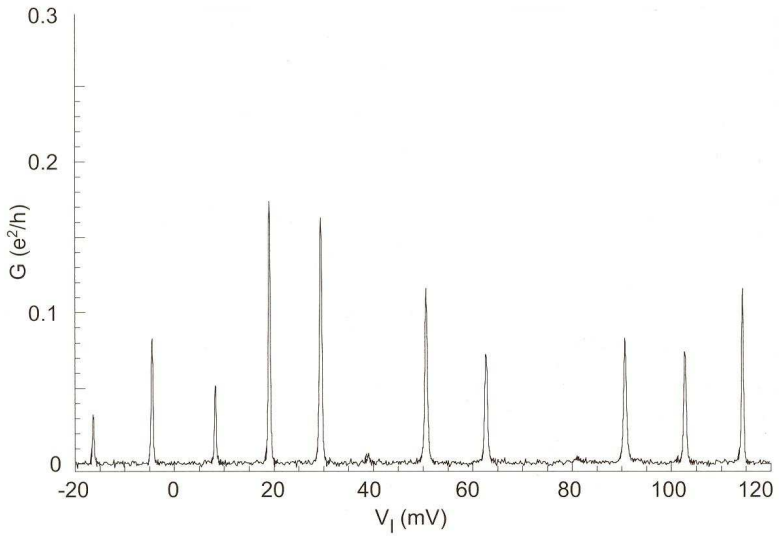

Figure 1.3.4: Conductance through an island as a function of the gate potential. We clearly see that current mostly flows at certain gate potentials. From [8].

if we measure the conductance of a typical quantum dot without any kind of filtering device we would observe more noise and imperfection than what is shown in Figure 1.3.4. Typically one would have main peaks which arise due to Coulomb blockage and noise which has to do with the size quantization. Also, when the gate potential increases we often see that we get closer spaced peaks. One explanation for this is that the dot increases in size, approaching the electrodes which increases conductance. The first peak can be the first electron on the dot, but it can also be the tenth. It depends on how we have tuned the tunnel barriers. When the barriers are sufficient close to the confining center for tunneling to happen, we normally see the first electron in the leftmost peak. If the distance is larger, we need to increase the radius of the electron cloud sitting in the center of the confinement. Since electrons repel each other, each time we add an electron, the size of the confined cloud increases and hence the distance to the tunnel barriers decrease. Since a increase in temperature adds more thermal fluctuations, the width of the peaks are directly related to the temperature of the sample. The Coulomb blocking is also a purely classical effect, but is affected by quantum mechanics at the QPC.

Observing Coulomb blockage in real life is not easy. First of all, the resistance in the QPC need to be sufficiently large. We need to observe single electrons tunneling through the QPC. This means, that the tunneling event time dt need to be significantly larger than the tunneling time τ. The tunneling time has been estimated as $\tau = \hbar/eV$ [15]. Now, if we estimate the tunneling event time

$$V = RI. \tag{1.5}$$

The current is known as dq/dt, which gives

$$dt = \frac{Rdq}{V}. \tag{1.6}$$

As the difference in charge is e, we simply get a crude approximate for the tunneling event time as

$$dt = Re/V. \tag{1.7}$$

Now, to observe a single electron transfer we would like to have $dt \gg \tau$, that is

$$R \gg \frac{\hbar}{e^2} \tag{1.8}$$

The temperature is also an important aspect. If the operational temperature is to high, we can have thermal fluctuations and excitations. Since we need a large tunnel resistor we quickly run into practical problems with cooling. Today, these limitations are seldom a problem and quantum dots made out of silicon is able to operates at room temperature.

The quantum dot will be exposed to magnetic field, either by design or accidentally. Hence, it is very important to know the inner workings when we apply a magnetic field. In most cases this is done in a way that the magnetic vector $\vec{B}$ is normal to the dot surface. For a typical quantum dot there is a complicated spectra of energy levels shown in Figure 1.3.5 In the next section

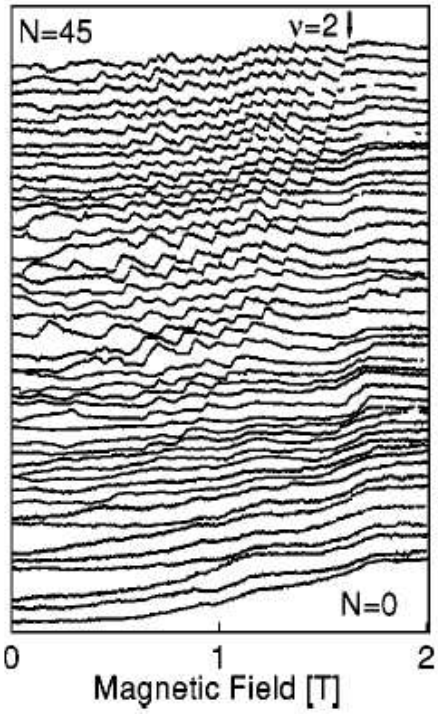

Figure 1.3.5: Energy as a function of magnetic field along normal plane of a quantum dot. These are typical experimental values. From [3].

we try to give a fist take of the theory behind some of the mentioned effects.

1.4 Single electron quantum dot

Quantum dots are complex devices. It is not easy to give a simple, yet complete theoretical explanation. Effects of electron-electron interactions, the Pauli exclusion principle, edge effects and external fields all need to be accounted for. And combinations are also possible. For a two-electron quantum dot, we only need to account for the two body interaction. However, as the electron number increase many body interaction occur and advanced band structures is revealed much due to a balance between the Pauli principle and electron-electron interaction.

Now, to start of, let us look at a quantum dot confined with a harmonic oscillator potential, making restrictions in the x-y directions, while we let the third dimension be locked down. This is typically done with a manufacture technique. We will also apply a constant magnetic field along this third dimension axis. This is of course an oversimplified case, but illustrates the ideas of the general description in three dimensions well.

1.4.1 Two dimensions

The two dimensional Hamilton operator for free electrons in a harmonic oscillator potential is

$$H = \sum_{i=1}^{N} \left(\frac{p_i^2}{2m^*} + \frac{1}{2} m^* \omega_0^2 (x_i^2 + y_i^2) \right), \tag{1.9}$$

where the electron number is N, the reduced electron mass m^* and the electron momentum p_i. The coordinates are given as x_i and y_i. By introducing a external vector field $\vec{A}$ we get a modified Hamiltonian

$$H = \sum_{i=1}^{N} \left(\frac{1}{2m^*} (\vec{p_i} + \frac{e}{c}\vec{A}_i)^2 + \frac{1}{2} m^* \omega_0^2 (x_i^2 + y_i^2) + e\phi + \vec{\rho}_i \cdot \vec{B} \right). \tag{1.10}$$

In addition to the added vector potential, we get a contribution from the electrical potential ϕ and the magnetic field B. The electron charge is e. The magnetic moment ρ is introduced due to the spin coupling with magnetic fields. The magnetic moment is known as $\vec{\rho} = q\vec{L}/2m$. However, since it is the electron spin that couples, we write $\vec{\rho} = -eg\vec{S}/2m^*c$, where g is the Landé g-factor. Since the two last terms in the Hamiltonian in Equation (1.10) are scalars and not operators, they can be taken outside and disregarded during calculations. We can reintroduce them in the final result if we want. We also see that Equation (1.10) is separable in single electron Hamiltonians. From now one we only consider the Hamiltonian for one electron. Let us look closer at Eq. (1.10). Without the scalar terms we have

$$H = \frac{1}{2m^*} (\vec{p} + \frac{e}{c}\vec{A})^2 + \frac{1}{2} m^* \omega_0^2 (x^2 + y^2), \tag{1.11}$$

expanding the first term gives

$$(\vec{p}+\frac{e}{c}\vec{A})^2 = p^2 + \frac{e}{c}\left(\vec{p}\cdot\vec{A}+\vec{A}\cdot\vec{p}\right)+\frac{e^2}{c^2}A^2. \tag{1.12}$$

The momentum and vector field does not commute general. However, by selecting a proper gauge they do. See Appendix A.2 for details. Since we want a constant magnetic field along the z-axis we can for example chose

$$\vec{A} = \frac{B}{2}\{-y, x, 0\}, \tag{1.13}$$

where B now is the amplitude of the applied magnetic field. By Maxwell's equations we have

$$\vec{B} = \nabla \times \vec{A}, \tag{1.14}$$

which gives

$$\vec{B} = B\vec{e}_z. \tag{1.15}$$

We see that the chosen $\vec{A}$ is valid. Putting the vector field from Eq. (1.13) into Eq. (1.12), we get

$$(\vec{p}+\frac{e}{c}\vec{A})^2 = p^2 + \frac{eB}{c}(xp_y - yp_x) + \frac{e^2B^2}{4c^2}\left(x^2+y^2\right). \tag{1.16}$$

Remember that we are using the Coulomb gauge. As a result $\vec{p}$ and $\vec{A}$ commutes. Substitute this back into Eq. (1.11) gives

$$H = \frac{1}{2m^*}\left(p^2 + \frac{eB}{c}(xp_y - yp_x) + \frac{e^2B^2}{4c^2}\left(x^2+y^2\right)\right) + \frac{1}{2}m^*\omega_0^2(x^2+y^2). \tag{1.17}$$

Where the second expression can be associated with the z-component of the angular momentum. See Appendix A.3. Now, if we define

$$\omega_B = \frac{eB}{2m^*c}, \tag{1.18}$$

and

$$\omega^2 = \omega_0^2 + \omega_B^2, \tag{1.19}$$

together with the substitution $p \to -i\hbar\nabla$. We get a more compact notation of the Hamilton. Also note that for example $p_x \to -i\hbar\partial/\partial x$

$$H = -\frac{1}{2m^*}\left(\hbar^2\nabla^2 + \frac{ie\hbar B}{c}(x\frac{\partial}{\partial y} - y\frac{\partial}{\partial x})\right) + \frac{1}{2}m^*\omega^2(x^2+y^2). \tag{1.20}$$

Changing to polar coordinates r and θ. Details for the transformation are given in Appendix A.3

$$H = -\frac{\hbar^2}{2m^*}\left(\frac{\partial^2}{\partial r^2} + \frac{1}{r}\frac{\partial}{\partial r} + \frac{1}{r^2}\frac{\partial^2}{\partial\theta^2} + i\frac{eB}{\hbar c}\frac{\partial}{\partial\theta}\right) + \frac{1}{2}m^*\omega^2 r^2 \tag{1.21}$$

At first sight changing to polar coordinates r and θ seem more complicated, but it is not. Doing this, we will end up solving a rather simple one dimensional

equation. Now is the time to bring in the Schrödinger equation

$$H\Psi = E\Psi \tag{1.22}$$

With the Hamiltonian in our case we now have the equation

$$-\frac{\hbar^2}{2m^*}\left(\frac{\partial^2}{\partial r^2}+\frac{1}{r}\frac{\partial}{\partial r}+\frac{1}{r^2}\frac{\partial^2}{\partial\theta^2}+i\frac{eB}{\hbar c}\frac{\partial}{\partial\theta}\right)\Psi(r,\theta)+\frac{1}{2}m^*\omega^2r^2\Psi(r,\theta)=E\Psi(r,\theta) \tag{1.23}$$

This equation is separable in R and θ. We can then assume

$$\Psi(r,\theta)=e^{im\theta}\psi(r), \tag{1.24}$$

Where m takes certain values, since $\theta+2\pi=\theta$, at least physically. This gives restrictions such that $m=0,\pm1,\pm2,...$ Substitute this into Eq. (1.23) results in the following Schrödinger equation

$$-\frac{\hbar^2}{2m^*}\left(\frac{\partial^2}{\partial r^2}+\frac{1}{r}\frac{\partial}{\partial r}-\frac{m^2}{r^2}-\frac{emB}{\hbar c}\right)\psi(r)+\frac{1}{2}m^*\omega^2r^2\psi(r)=E\psi(r) \tag{1.25}$$

The eigenvector to this equation is given as

$$\psi(r)_{nm}=\sqrt{\frac{2n!}{(n+|m|)!}}\beta^{(|m|+1)/2}r^{|m|}e^{-\beta r^2/2}L_n^{|m|}(\beta r^2), \tag{1.26}$$

with the eigenvalues

$$E=(2n+|m|+1)\hbar\omega+m\hbar\omega_B. \tag{1.27}$$

See Appendix A.6.1 for derivation of both. Now, if we use Eq. (1.19) we can rewrite Eq. (1.27) to get

$$\frac{E}{\hbar\omega_0}=(2n+|m|+1)\sqrt{1+\frac{\omega_B^2}{\omega_0^2}}+m\frac{\omega_B}{\omega_0}. \tag{1.28}$$

This equation give rise to the Fock-Darwin energy spectrum showed in Figure 1.4.6. At $B=0$, in this case where $\omega_B=0$, the eigenvalues are

$$E^{B=0}\approx(2n+|m|+1)\hbar\omega_0, \tag{1.29}$$

the degeneracy of these levels are $d=2n+|m|+1$. If we now define a new quantum number, say $N=2n+|m|$ we can develop shell fillings shown in Tab. 1.4.2. Remember that due to the electron spin degeneracy we have a additional degeneracy of a factor 2 on top of the previous mentioned degeneracy. The total degeneracy can then be defined as $D=2d$. This extra degeneracy is not shown in Fig. 1.4.6 since we excluded the electron spin coupling in the energy term from Eq. (1.27). In the large field limit, where $\omega_B\to\infty$ we get the energy levels

$$E^{B\to\infty}\approx(2n+|m|+m+1)\hbar\omega_B. \tag{1.30}$$

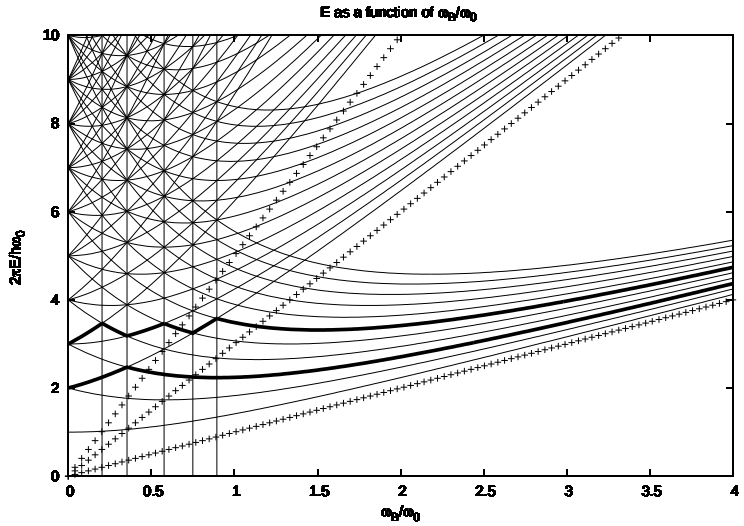

Figure 1.4.6: Two dimensional Fock-Darwin energy spectrum. Landau levels are clearly visible at the far right in the figure

N	D=2d	Shell filling=S
0	2	2
1	4	6
2	6	12
3	8	20

Table 1.4.2: Two dimensional quantum numbers and shell filling for a quantum dot without electron-electron interaction. The shell filling factor tells us how many electrons there is in the dot, up to the given state N

Observe that we have two cases, one for $m \geq 0$ and $m < 0$. For the first case, the energy can be given as

$$E^{B\to\infty} \approx (2(n+m)+1)\hbar\omega_B, \tag{1.31}$$

while in the second case, the m terms cancel and we are left with

$$E^{B\to\infty} \approx (2n+1)\hbar\omega_B. \tag{1.32}$$

Notice that in both cases the energy is odd. By defining the Landau level quantum number $N_L = 0, 1, 2, ...$, we can write the high field approximation as

$$\frac{E^{B\to\infty}}{\hbar\omega_0} \approx (2N_L+1)\frac{\omega_B}{\omega_0}. \tag{1.33}$$

These energy lines are shown in Fig. 1.4.6 as dotted lines for $N_L = 0, 1, 2$. We clearly see that as the magnetic field is increased the Fock-Darwin spectrum approaches Landau levels. It is actually more correct to call them Landau bands,

since they can have an infinite degeneracy due to the negative m canceling in the energy. In real life, this is not infinite due to i.e. limited size of the samples and number of particles on the dot. The intersection points are highlighted using vertical lines in Fig. 1.4.6. They will appear where the ratio of energy difference between two Landau levels and sublevels are an integer. In Fig. 1.4.6 we have only calculated and drawn a limited number of landau levels and sublevels, but it is enough to illustrate what will happen to a energy level when the magnetic field is increased. First, nothing happens, the energy of the electron increase, but suddenly accidental degeneracy occur and the electron choose the state which is most favorable to minimize the energy. We then get zig-zag lines indicated in Fig 1.4.6. They are very important and show up in experiments. They can to some extent predict the conductance peaks mentioned in Sec. 1.3, but it is by no means a perfect model. We can relate the two bold lines in Fig. 1.4.6 to filled shelled, for $S = 6$ and $S = 12$ particles. When the quantum dot is in a filled shell status, we need to add energy to open up a new shell, and place electrons such that they obey the Pauli principle. It takes much less energy to add an electron to an already open shell. From Fig. 1.3.5 we can see similarities, however deviations are clearly visible. This should not come as a surprise, since the model seem overly simplified and electron-electron interaction is left out.

In the beginning of this section we disregarded some constant terms to simplify calculations. Since we have set $\vec{E} = \vec{0}$, the term left out take care of the energy difference due to the coupling between the electron spin and the magnetic field. Including this term in the energy gives,

$$E = (2n + |m| + 1)\hbar\omega + m\hbar\omega_B + gs\hbar\omega_B. \tag{1.34}$$

The Landé g-factor, g can be located in recent constant tables for particle physics (FINN REF). It was first believed to be $g = 2$, but nowadays this is incorrect. It is close, but not entirely. The electron spin, s can take half integer values, $s = \pm 1/2$. In real life experiments it is almost impossible to restrict the quantum dot in one direction. We will now look at three dimensions and how this relates to the previously discussed two dimensional case.

1.4.2 Three dimensions

The three dimensional case follow Sec. 1.4.1 until we write out the Hamiltonian in Eq. (1.20). The only difference is that we in addition get an extra z^2 term from the harmonic oscillator. The new Hamiltonian in three dimensions reads

$$H = -\frac{1}{2m^*}\left(\hbar^2\nabla^2 + \frac{ie\hbar B}{c}(x\frac{\partial}{\partial y} + y\frac{\partial}{\partial x})\right) + \frac{1}{2}m^*\omega^2(x^2 + y^2 + z^2). \tag{1.35}$$

If we did not have the z-component due to the harmonic confinement, the only z dependent term would be p_z. We could then separate the Schrödinger equation in z and (x, y). This is not the case here, since p_z and z does not commute. So we will have to develop a new solution from this point. The ∇^2 operator in spherical coordinates and the derivatives are given in Ap. A.3. Substituting

this into Eq. (1.35) gives

$$H = -\frac{1}{2m^*} \quad \left\{ \quad \hbar^2 \left(\frac{\partial^2}{\partial r^2} + \frac{2}{r}\frac{\partial}{\partial r} + \frac{1}{r^2}\left(\frac{1}{sin^2(\phi)}\frac{\partial^2}{\partial \theta^2} + cot(\phi)\frac{\partial}{\partial \phi} + \frac{\partial^2}{\partial \phi^2} \right) \right) \right.$$
$$\left. + \quad \frac{ie\hbar B}{c}\frac{\partial}{\partial \theta} \right\} + \frac{1}{2}m^*\omega^2 r^2. \tag{1.36}$$

We observe that the angle dependent part in the brackets are the L^2 operator and the single derivative on θ are related to L_z. Refer to Ap. A.3 for details. From the Schrödinger equation

$$H\Psi = E\Psi, \tag{1.37}$$

we can asume

$$\Psi(r, \theta, \phi) = \psi(r)\Omega(\theta, \phi). \tag{1.38}$$

The solutions of the angle dependent eigenvalue and eigenvector are worked out in several textbooks describing quantum mechanics. See for example [19] . The eigenvalues of L_z and L^2 are given as

$$L^2\Omega(\theta, \phi) = \hbar^2 l(l+1)\Omega(\theta, \phi), \tag{1.39}$$

$$L_z\Omega(\theta, \phi) = m\hbar\Omega(\theta, \phi), \tag{1.40}$$

where $l = 0, 1, 2, ...$ and $m = 0, \pm 1, \pm 2, ...$ The solution to the eigenvectors $\Omega(\theta, \phi)$ are

$$\Omega(\theta, \phi)_{lm} = \alpha_m \sqrt{\frac{(2l+1)(l+|m|)!}{4\pi(l-|m|)!}} P_l^{|m|}(cos(\phi))e^{im\phi}, \tag{1.41}$$

with the definition

$$\alpha_m = \begin{cases} 0 & m \leq 0 \\ (-1)^m & m \geq 0 \end{cases} \tag{1.42}$$

In the derivation the limitation $|m| \leq l$ is developed to obtain valid solutions. The Legendre polynomials $P_l^{|m|}(x)$ are tabulated in (FINN REF). The first few are listed in Tab. 1.4.3. They are defined by the Rodrigues representation

$$P_l^{|m|}(x) = \frac{(-1)^{|m|}}{2^l l!}(1-x^2)^{\frac{|m|}{2}} \left(\frac{d}{dx} \right)^{l+|m|} (x^2-1)^l, \tag{1.43}$$

and the recurrence relation

$$P_l^{|m|}(x) = \frac{1}{l-|m|}\Big(x(2l-1)P_{l-1}^{|m|}(x) - (l+|m|-1)P_{l-2}^{|m|}(x) \Big) \tag{1.44}$$

We put the solutions back into the Hamiltonian in Eq. (1.36) and use the Schrödinger equation to get

$$-\frac{\hbar^2}{2m^*}\left\{ \frac{\partial^2}{\partial r^2} + \frac{2}{r}\frac{\partial}{\partial r} - \frac{l(l+1)}{r^2} - \frac{emB}{\hbar c} \right\}\psi(r) + \frac{1}{2}m^*\omega^2 r^2\psi(r) = E\psi(r). \tag{1.45}$$

$\|m\|$	l	$P_l^{\|m\|}(x)$
0	0	1
0	1	x
0	2	$\frac{1}{2}\left(3x^2-1\right)$
1	1	$-\sqrt{1-x^2}$
1	2	$-3x\sqrt{1-x^2}$
2	2	$3(1-x^2)$

Table 1.4.3: Lowest order associated Legendre polynomials.

Comparing this equation with Eq. (1.25) we see similarities. The eigensolutions of Eq. (1.45) are found in Ap. A.6.2. The eigenvalues are

$$E = \left(2n + l + \frac{3}{2}\right)\hbar\omega + m\hbar\omega_B. \tag{1.46}$$

If we divide both sides by $\hbar\omega_0$ we get

$$\frac{E}{\hbar\omega_0} = \left(2n + l + \frac{3}{2}\right)\sqrt{1 + \frac{\omega_B^2}{\omega_0^2}} + m\frac{\omega_B}{\omega_0}. \tag{1.47}$$

Due to the limitation $|m| \leq l$ each l will give rise to a degeneracy of $2l+1$. As in the two dimensional case we define $N = 2n + l$. This give rise to the same behavior as the Fock-Darwin spectrum in Sec. 1.4.1, but with added degeneracy. See Fig.1.4.7 for details. The filled shells can be located in the Fock-Darwin spectrum as described in Sec. 1.4.1. The filled shells and the degeneracy factors

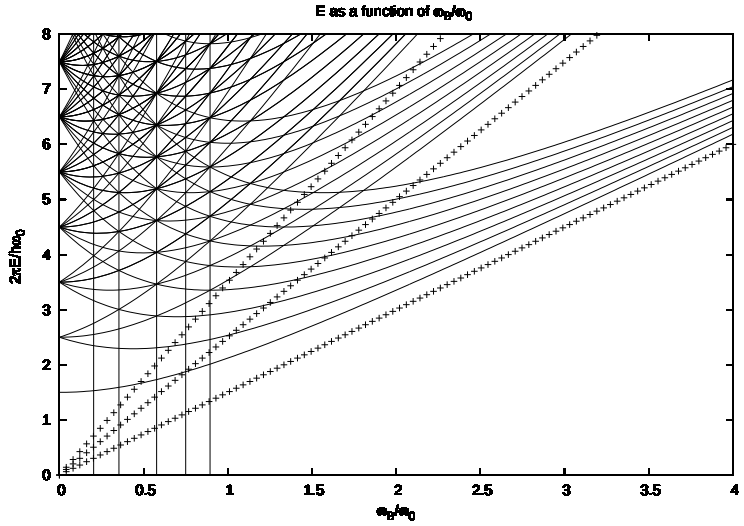

Figure 1.4.7: Three dimensional Fock-Darwin energy spectrum. Landau levels are clearly visible at the far right in the figure

are tabulated for the lowest states in Tab. 1.4.4. The total degeneracy D is obtained by adding the spin degeneracy of the electrons.

N	D=2d	Shell filling=S
0	2	2
1	6	8
2	12	20
3	20	40

Table 1.4.4: Three dimensional quantum numbers and shell filling for a quantum dot without electron-electron interaction. The shell filling factor tells us how many electrons there is in the dot, up to the given state N

The last two sections shed light on some of the effects seen in quantum dots. It is not a complete model and in the next section we will look at the electron-electron interaction.

1.5 Two electron quantum dot

Let us now consider two body interactions. Since the mass is equal for the two particles we only include the constant correction and keep m^* as the single electron mass therm during all calculation unless otherwise stated. However the electron mass in an electron gas or in solids are not the same as in the free case, therefore the reduced mass m^*. It is possible to calculate a reduced mass for the electron in different medium, see (FINN REF). The Hamiltonian we are to consider have the following structure.

$$\begin{aligned} H = \sum_{i=1}^{2} & \left\{ \frac{1}{2m^*}\left(\vec{p}_i + \frac{e}{c}\vec{A}_i\right)^2 + \frac{1}{2}m\omega_0^2 r_i^2 \right. \\ & + \left. e\phi + \vec{\rho}_i \cdot \vec{B} \right\} + \frac{e^2}{4\pi\epsilon\epsilon_0}\frac{1}{|\vec{r}_1 - \vec{r}_2|} \end{aligned} \tag{1.48}$$

Again the scalars can be included in the eigenvalues. We therefore ship their discussion until further notice. For simplicity we still want to consider a constant magnetic fields along the z-axis. Just as before, we choose

$$\vec{A} = \frac{B}{2}\{-y, x, 0\}. \tag{1.49}$$

The major problem of equation Eq. (1.48) is the interacting therm. There are few workarounds for this, but introducing relative and center-of-mass coordinates is a successful method. Defining

$$\vec{r} = \vec{r}_1 - \vec{r}_2, \tag{1.50}$$

$$\vec{R} = \frac{1}{2}(\vec{r}_1 + \vec{r}_2), \tag{1.51}$$

where $\vec{R}$ and $\vec{r}$ represent the center-of-mass and relative coordinates.

$$\vec{p} = \frac{1}{2}(\vec{p}_1 - \vec{p}_2), \tag{1.52}$$

$$\vec{P} = \vec{p}_1 + \vec{p}_2. \tag{1.53}$$

Remember that we choose $\vec{B}$ to be a constant. The angular momentum $\vec{l} = \vec{r} \times \vec{p}$ can now be expressed. Let us define $\vec{L}$, $\vec{ll}$, $\vec{l_1}$ and $\vec{l_2}$ as the angular momentum for the center-of-mass, relative, particle one and particle two respectively. Angular momenta for the center-of-mass motion is

$$\vec{L} = \vec{R} \times \vec{P}, \tag{1.54}$$

using Eq. (1.51) and 1.53 yields

$$\vec{L} = \frac{1}{2}\left\{\vec{r_1} \times \vec{p_1} + \vec{r_2} \times \vec{p_1} + \vec{r_1} \times \vec{p_2} + \vec{r_2} \times \vec{p_2}\right\}. \tag{1.55}$$

Similarly we get

$$\vec{l} = \frac{1}{2}\left\{\vec{r_1} \times \vec{p_1} - \vec{r_2} \times \vec{p_1} - \vec{r_1} \times \vec{p_2} + \vec{r_2} \times \vec{p_2}\right\} \tag{1.56}$$

$$\vec{l_1} = \vec{r_1} \times \vec{p_1} \tag{1.57}$$

$$\vec{l_2} = \vec{r_2} \times \vec{p_2}. \tag{1.58}$$

Adding the relative and center-of-mass angular momenta gives the relation

$$\vec{l_1} + \vec{l_2} = \vec{l} + \vec{L}. \tag{1.59}$$

In other words, the total angular momenta is conserved during the coordinate transformation.

Obeying Maxwell's equations leads to the requirement that $\vec{A}$ should be linear. The $\vec{A}$ field uses coordinates as variables and substituting the previous definitions we find

$$\vec{A}(\vec{r}) = \vec{A}(\vec{r}_1) - \vec{A}(\vec{r}_2), \tag{1.60}$$

$$\vec{A}(\vec{R}) = \frac{1}{2}\left(\vec{A}(\vec{r}_1) + \vec{A}(\vec{r}_2)\right). \tag{1.61}$$

We now want to transform Eq. (1.48) to the new coordinates. The Hamiltonian before the minimal substitution have the form

$$H_{pre} = \sum_{i=1}^{2}\left\{\frac{1}{2m^*}p_i^2 + \frac{1}{2}m^*\omega_0^2 r_i^2\right\} + \frac{e^2}{4\pi\epsilon_0\epsilon}\frac{1}{|\vec{r}_1 - \vec{r}_2|}. \tag{1.62}$$

Expanding and substituting we see that

$$p_1^2 + p_2^2 = \frac{1}{2}\left(P^2 + 4p^2\right), \tag{1.63}$$

$$r_1^2 + r_2^2 = \frac{1}{2}\left(4R^2 + r^2\right), \tag{1.64}$$

$$|\vec{r}_1 - \vec{r}_2| = r. \tag{1.65}$$

This give us the new separated Hamiltonian

$$H_{pre} = 2H_r + \frac{1}{2}H_R, \tag{1.66}$$

where

$$\begin{aligned} H_r &= \frac{p^2}{2m^*} + \frac{1}{2}m^*\omega_r^2 r^2 + \frac{e^2}{8\pi\epsilon_0\epsilon r}, && (1.67)\\ H_R &= \frac{P^2}{2m^*} + \frac{1}{2}m^*\omega_R^2 R^2, && (1.68)\\ \omega_r &= \frac{\omega_0}{2}, && (1.69)\\ \omega_R &= 2\omega_0. && (1.70) \end{aligned}$$

Where H_r and H_R are the Hamiltonian operators for the relative and center-of-mass respectively. If we do the minimal substitution with new variables $\vec{A}_r$ and $\vec{A}_R$ for the potentials we get the equation

$$H = \frac{(\vec{P} + \vec{A}_R)^2}{4m^*} + m^*\omega_0^2 R^2 + \frac{(\vec{p} + \vec{A}_r)^2}{m^*} + \frac{1}{4}m^*\omega_0^2 r^2 + \frac{e^2}{4\pi\epsilon_0\epsilon}\frac{1}{r} \tag{1.71}$$

If we write out this equation and compare it to equation Eq. (1.48) we see that it is convenient to relate the new potentials as

$$\begin{aligned} \vec{A}_r &= \frac{1}{2}\vec{A}(\vec{r}), && (1.72)\\ \vec{A}_R &= 2\vec{A}(\vec{R}). && (1.73) \end{aligned}$$

By doing this, we get the same scaling factors in front of the potentials as in the kinetic terms. We can now write out the Hamiltonian of the interacting electrons. Just as in Section 1.4 we have skipped the scalar terms.

$$\begin{aligned} H &= 2H_r + \frac{1}{2}H_R + H_S, && (1.74)\\ H_R &= \frac{\left(\vec{P} + \vec{A}_R\right)^2}{2m^*} + \frac{1}{2}m^*\omega_R^2 R^2, && (1.75)\\ H_r &= \frac{\left(\vec{p} + \vec{A}_r\right)^2}{2m^*} + \frac{1}{2}m^*\omega_r^2 r^2 + \frac{e^2}{8\pi\epsilon_0\epsilon r}. && (1.76) \end{aligned}$$

In Eq. (1.74) we have included an extra term called H_S. This is the Hamilton operator for the spin coupling to the magnetic field. When a spin is chosen this operator is a scalar. The form of H_S can be seen in Eq. (1.10) as the last term. Using the Schrödinger equation

$$H\Psi = E\Psi, \tag{1.77}$$

with the Hamilton operator defined in Eq. (1.74) we can write the eigenvectors as

$$\Psi = \Phi(r)\Upsilon(R)\chi(s_1, s_2), \tag{1.78}$$

where $\Psi(r)$, $\Upsilon(R)$ and $\chi(s_1, s_2)$ are the eigenfunctions for the relative, center-of-mass and spin part respectively. The corresponding eigenvalues are

$$E = 2\epsilon_r + \frac{1}{2}\epsilon_R + \epsilon_{adj}, \tag{1.79}$$

where the last term includes the eigenvalue of H_S and the other scalar terms discussed in Section 1.4. We can separate the solutions like this, since the Hamilton operator in Eq. (1.74) commutes with its siblings. The eigensolutions of the center-of-mass part is just as for the one particle case, with modified parameters. The two dimensional solutions are worked out in Section 1.4 and will not be discussed until further notice. We will now only focus on the relative part until we bring everything together at the end. It turns out that there exist solutions for the relative part which are exact, but they are very special. The solutions are worked out in Appendix A.7. In the general case we need to solve the differential equations numerically. This is what we cover in the next section.

2 Interacting electrons and diagonalization

We will in this section switch to Dirac notation. See basic textbooks on quantum mechanics i.e.[19] for a mathematical introduction to Dirac notation. We will also make use of Einstein summations (FINN REF) to make the notation as compact as possible. Up until now, we had the possibility to solve the Schrödinger equations analytically. The two and three dimensional solutions of Eq. (1.77) can only be solved generally by numerical methods. The equations can be solved exact up to numerical limitations. The limitations lies in the accuracy, size and computing time. Using Dirac notation we can now write Eq. (1.77) as

$$H|\beta_1\beta_2\beta_3...\rangle = E|\beta_1\beta_2\beta_3...\rangle. \tag{2.80}$$

Where we use H from Eq. (1.74) and E as the eigenvalue corresponding to the given Hamiltonian. The quantum numbers β_i describing the different states are at this point unknown. By defining $\beta = \beta_1\beta_2\beta_3...$ we get a more compact notation. The eigenvectors $|\beta\rangle$ form a basis in the Hilbert space (FINN REF) and are orthonormal

$$\langle\beta'|\beta\rangle = \delta_{\beta'\beta}. \tag{2.81}$$

Multiplying Eq. (2.80) with $\langle\beta'|$ from the left we get

$$\langle\beta'|H|\beta\rangle = E, \tag{2.82}$$

where the left side are matrix components

$$H_{\beta'\beta} = \langle\beta'|H|\beta\rangle. \tag{2.83}$$

To find the eigenvalues we need to diagonalize the matrix. This is done by orthogonal transformations. The methods used in this thesis use what is called QR algorithm with implicit shifts and Householder reduction. The derivation of these methods are outlined in [7] and [14]. In the first section we will solve the Hamilton operator from Eq. (1.74) in both two and three dimensions. This is done exact, using numerical derivatives. Then in the next section we will

diagonalize the same Hamilton operator using the harmonic oscillator as a basis. At the end we will compare the two solutions and do perturbation theory in addition. This will give a convenient overview of the different solutions.

2.1 Diagonalization in the harmonic oscillator basis

In Ap. A.6.1 we calculated the exact harmonic oscillator basis functions for two dimensions. We saw that we only have two quantum numbers, n and m respectively. The Schrödinger equation in harmonic oscillator basis can be written

$$H|NMnm\rangle = E|NMnm\rangle. \tag{2.84}$$

Where we use the Hamiltonian and the eigenvalues from Eq. (1.74) and Eq. (1.79). The large capitol quantum numbers represent the center-of-mass basis, while the small represent the relative basis. Multiplying from the left with $\langle N'M'n'm'|$ gives

$$E = \langle N'M'n'm'|H|NMnm\rangle. \tag{2.85}$$

In the rest of this section we disregard the spin coupling H_S and the addition energy ϵ_{adj} from Eq. (1.74) until further notice. From Eq. (1.74) we can now write

$$E = 2\langle N'M'n'm'|H_r|NMnm\rangle + \frac{1}{2}\langle N'M'n'm'|H_R|NMnm\rangle. \tag{2.86}$$

The relative Hamiltonian does not operate on the center-of-mass eigenfunctions. One often say that H_r is diagonal in N, N', M and M'. Vice-versa for the center-of-mass Hamiltonian. Using this, we can write Eq. (2.86) as

$$E = 2\langle n'm'|H_r|nm\rangle + \frac{1}{2}\langle N'M'|H_R|NM\rangle. \tag{2.87}$$

The last term is the center-of-mass energy. The center-of-mass solutions are exactly the same as the solutions worked out in Ap. A.6.1, but with capital quantum numbers. We can simplify Eq. (2.87) even more. The relative motion is the same as the center-of-mass motion, but with the addition of the Coulomb interaction. We can then define $H_r = H_{r_0} + H_{r_1}$ where H_{r_1} describes the Coulomb interaction part of H_r while H_{r_0} is equal to H_R with the coordinates replaced by r. Then H_{r_1} will be diagonal in m and m'. We can now write the first term in Eq. (2.87) as

$$\epsilon_r = (2n + |m| + 1)\hbar\omega + \langle n'm|H_{r_1}|nm\rangle. \tag{2.88}$$

The relative energy are defined in Eq. (1.79). The only term we need to calculate when using the Harmonic oscillator basis are the matrix elements

$$\langle n'm|H_{r_1}|nm\rangle_{n'n} = \int_V \Psi^*_{n'm}\Psi_{nm}\frac{\sigma}{r}dV. \tag{2.89}$$

Observe the symmetry when we exchange n' and n. The constant $\sigma = e^2/8\pi\epsilon\epsilon_0$ determines the strength of the interaction, while Ψ describe the eigenfunctions. We have dropped the coordinate dependence since they differ in two and three dimension. For the two dimensional case, this expression becomes rather easy

to calculate. The angle dependent part completely cancel and we are left with an integral over the harmonic oscillator eigenfunction calculated in Sec. A.6.1. Putting these functions into Eq. (2.89) together with the volume element from Sec. A.3 we get

$$\langle n'm|H_{r_1}|nm\rangle^{2D}_{n'n} = \int_0^\infty \psi_{nm}(r)\psi_{n'm}(r)\frac{\sigma}{r}rdr. \tag{2.90}$$

The $1/r$ Coulomb dependence cancel with the volume element. In three dimension this expression is the same apart from the extra r factor and another set of basis functions calculated in Sec. A.6.2.

The quantum numbers have no upper limit and the matrix elements will be infinite large matrices. To obtain eigenvalues we need to diagonalize the matrix. This is done on a computer using matrix manipulation techniques. Obviously, infinite matrices cannot be threated and we need to introduce a cut-off on the quantum numbers. It is very important that this cut-off does not affect the eigenvalues we are to consider. In this thesis, we only consider the lowest eigenvalues, but we still need to determine a sufficiently high cut-off.

We need to calculate Eq. (2.89) in an effective way. The obvious solution is to use a numerical integration techniques. Let us first develop an explicit expression for the integral in two dimensions. Substituting the basis function in Sec. A.6.1 into Eq. (2.90) we get

$$\langle n'm|H_{r_1}|nm\rangle^{2D}_{n'n} = \sigma\int_0^\infty \beta^{|m|+1}r^{2|m|}e^{-\beta r^2}L^{|m|}_{n'}(\beta r^2)L^{|m|}_{n}(\beta r^2)dr. \tag{2.91}$$

Substitute $x = \beta r^2$ gives

$$\langle n'm|H_{r_1}|nm\rangle^{2D}_{n'n} = \frac{\sigma\sqrt{\beta}}{2}\int_0^\infty x^{|m|-1/2}e^{-x}L^{|m|}_{n'}(x)L^{|m|}_{n}(x)dx. \tag{2.92}$$

The constant term in front of the integral can be simplified by multiplying the fraction by $\omega m^*\hbar^3$ in the denominator and nominator. This give rise to a modified Bohr radius due to the reduced mass of the electron and the oscillator length l_0. Both of these are defined in Eq. (A.196) and (A.197) respectively. And then we divide the equation by $\hbar\omega$ and get

$$\frac{\langle n'm|H_{r_1}|nm\rangle^{2D}_{n'n}}{\hbar\omega} = \frac{l_0}{4a_0^*}I^{2D}_{n'n}, \tag{2.93}$$

where

$$I^{2D}_{n'n} = \sqrt{\frac{2n'!}{(n'+|m|)!}}\sqrt{\frac{2n!}{(n+|m|)!}}\int_0^\infty x^{|m|-1/2}e^{-x}L^{|m|}_{n'}(x)L^{|m|}_{n}(x)dx. \tag{2.94}$$

This a dimensionless integral and this suits a dimensionless form of the energy term in Eq. (2.88) perfectly. For three dimensions all the previous discussions apply. But there are important differences. The volume element is different. See Ap. A.3 for details. The quantum number m is replaced by $l - 1/2$ in addition to slight differences in the eigenfunctions. Taking this into account we get the

interacting energy in three dimensions as

$$\frac{\langle n'm|H_{r_1}|nm\rangle_{n'n}^{3D}}{\hbar\omega} = \frac{l_0}{4a_0^*} I_{n'n}^{3D}, \tag{2.95}$$

with I_{3D} defined as

$$I_{n'n}^{3D} = \sqrt{\frac{2n'!}{(n'+l+1/2)!}}\sqrt{\frac{2n!}{(n+l+1/2)!}}\int_0^\infty x^l e^{-x} L_{n'}^{l-1/2}(x) L_n^{l-1/2}(x) dx. \tag{2.96}$$

The interacting integrals for two and three dimensions cannot generally be solved analytically due to the Laguerre polynomials. But it's possible to express Eq. (2.89) as a series. We will now consider the two dimensional matrix elements in Eq. (2.90) and express the eigenfunction by a series over the Talmi integrals [20]. By doing this we can develop an analytic solution to Eq. (2.90) of any order in the quantum numbers without calculating the integral. We will follow [5] where the solutions for the three dimensional harmonic oscillator are worked out in detail. By using the alternative eigenfunction from Eq. (A.166) and the substitution $\rho^2 = \beta r^2$ we can now write Eq. (2.90) as

$$\langle n'm|H_{r_1}|nm\rangle_{n'n}^{2D} = \hbar\omega \sum_{k'=0}^{n'}\sum_{k=0}^{n} a_{n'mk'} a_{nmk} \frac{l_0}{2a_0^*}\int_0^\infty e^{-\rho^2}\rho^{2(k'+k+|m|)} d\rho. \tag{2.97}$$

If we now redefine $p = k + k' + |m|$ we can write the equation above in the following way

$$\langle n'm|H_{r_1}|nm\rangle_{n'n}^{2D} = \hbar\omega \frac{l_0}{2a_0^*}\sum_p B(n'm, nm, p) I_p. \tag{2.98}$$

We now have a series expansion of the B factors given as

$$B(n'm, nm, p) = \frac{\Gamma(p+3/2)}{2}\sum_{k=0}^{n} a_{nmk} a_{n'm(p-k-|m|)}, \tag{2.99}$$

where Γ is the Gamma function (FINN REF, mathworld) and I_p the Talmi integrals, defined as

$$I_p = \frac{2}{\Gamma(p+3/2)}\int_0^\infty \rho^{2p} e^{-\rho^2} d\rho. \tag{2.100}$$

The Talmi integrals are tabulated (I REF OVER?) and we find that

$$I_p = \frac{\Gamma(p+1/2)}{\Gamma(p+3/2)}. \tag{2.101}$$

The properties of Gamma function ensure that $\Gamma(n+1) = n\Gamma(n)$ (FINN REF). Using this, the equation above can be simplified to

$$I_p = \frac{1}{p+1/2}. \tag{2.102}$$

The coefficient B are tabulated and discussed in [1, 2] and can be found by the rather complicated expression listed in Ap. A.8.1. The summation over p are by the relation $p = k + k' + |m|$ only allowed to take the following values

$$|m| \leq p \leq n' + n + |m|. \tag{2.103}$$

We now obtained a simple way of generating the values of Eq. (2.97) by the use of numerics. The matrix elements are now given as

$$\frac{\langle n'm|H_{r_1}|nm\rangle_{n'n}^{2D}}{\hbar\omega} = \frac{l_0}{2a_0^*}\sum_p B(n'm, nm, p)\frac{1}{p+1/2}. \tag{2.104}$$

Both the integral and series method involves factorials. They increase with the matrix size and we need to determine the limits in the numerics. In modern computers double precision is the most common representation when large numbers or precision are needed. Double precision utilize 64-bit. For an overview on number representation see [9]. There exist arbitrary precision methods, but they greatly increase computation time. Hence they are not used in this thesis. The largest number we can represent using double precision are in the range of 10^{308}. This limit is reached for 170!. By looking at the normalization factors we see that the biggest factorials we need to calculate are $(n + |m|)!$ for two dimensions and $(n + l + 1/2)!$ for three dimensions. Note that we can write

$$(n + \frac{1}{2})! = \frac{\sqrt{\pi}}{2^{2n+1}}\frac{(2n+1)!}{n!}. \tag{2.105}$$

This yields an upper numerical limit of $n + |m| = 170$ and $n + l = 84$ in two and three dimension respectively for the integration method. For the series method we see from Eq. (A.167) and (A.186) that the upper limits due to the single factorial calculations are the same as for the integration method. But we are multiplying large factorials together in a brute force way, thus making it more severe. We have compared the two method in Fig. 2.1.8. The numerical integration was carried out by using Gauss-Laguerre. Why Gauss-Laguerre are used is explained in a moment. We clearly see the problems with the series method. In both two and three dimensions the normalization diverges as soon as we hit $n \approx 14$ for $m = 0$ and around $n \approx 12$ for $m = 5$. This seems a bit odd at first, but let us first address the brute force multiplication of factorials. Observe that we can write

$$\frac{a!\ b!}{c!} = e^{ln(a!)+ln(b!)-ln(c!)}. \tag{2.106}$$

This is a simple, yet clever way of expressing ratios of large factorials. In Fig. 2.1.9 we make use of this multiplication scheme. However, notice that there is not any noticeable difference between Fig. 2.1.8 and 2.1.9. By employing a totally different multiplication scheme for the factorials, we are left with the same behavior. If we take a look at the factorial products they are well withing the numerical limit at 10^{308} even for quite large n, taking $m = 0$. This predicts that the results of a change in multiplication scheme should not have any impact, as long as we are withing the numerical limits. The only operation not considered is the summation. For each increase in k or k' we change sign of

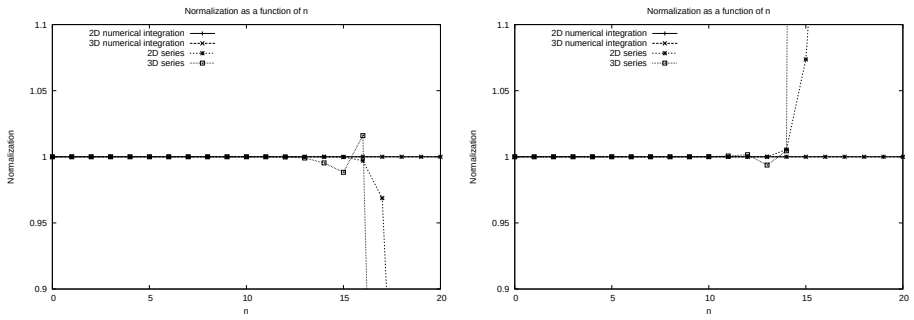

(a) $m, l = 0$ (b) $m, l = 5$

Figure 2.1.8: Normalization as function of n. Using brute force factorial multiplication. We clearly see instabilities.

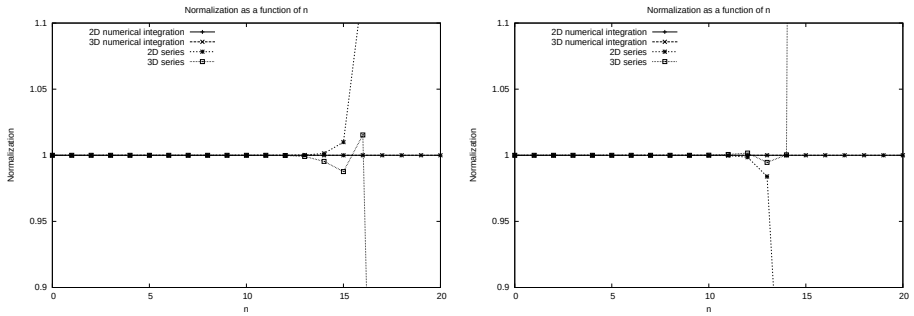

(a) $m, l = 0$ (b) $m, l = 5$

Figure 2.1.9: Normalization as function of n. Using multiplication scheme in Eq. (2.106). We see the same behavior as in Fig. fig:normalization.

the coefficient, thus leading to an alternating series. At the same time, k and k' are increasing, so we are summing larger and larger positive and negative numbers. To illustrate that this is the problem, we sum all the positive and negative numbers separately and take the sum of the totals at the end. By using the brute force multiplication scheme, Fig. 2.1.10 illustrates a slight improvement, at least for two dimensions. The series method needs sophisticated and maybe arbitrary precision techniques to give acceptable results at high n. Hence we will use numerical integration in this thesis. First we need to choose a fast and accurate numerical integration technique. In harmonic oscillator problems the Gauss-Laguerre technique are preferred. See App. A.5 for details. The number of different quantum numbers n' and n are restricted due to computer work. A method that punish computer accuracy rather than computer work should not be preferred. Due to finite computing time, we need to have an upper limit on n' and n. This upper limit needs to be determined before we continue. Ideally we want to set it very big, but even modern computers are severely limited when it comes to matrix calculations. We have introduced ϵ which we define as

$$\epsilon = E_{n_{max}} - E_{n'_{max}}. \tag{2.107}$$

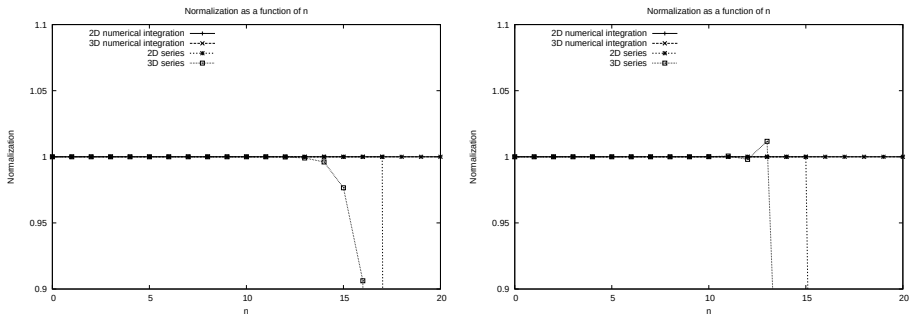

(a) $m, l = 0$ (b) $m, l = 5$

Figure 2.1.10: Normalization as function of n. Using brute force factorial multiplication, but with separate negative and positive summation. We see slight improvements over Fig. fig:normalization.

Where n_{max} is the matrix cutoff and $n'_{max} > n_{max}$. As we increase n_{max} more and more states are included in the diagonalization process. As the matrix grows large, the added row and column contributes less to the eigenvalues. Thus we should observe a convergence in ϵ as we increase n_{max}. The strength of the Coulomb interaction is determined by l_0/a_0. When the strength grows the off-diagonal elements grow and might give faster or slower convergence. For three dimensions these behaviors are observed in Fig. 2.1.11 and 2.1.12. For $l_0/a_0 = 1$ we have a slow convergence compared to the others, while $l_0/a_0 = 10$ seem to give the fastest convergence of the four. As n_{max} approaches 100, we see that we have convergence for all four values of l_0/a_0. Even at $n_{max} = 80$ the plots have a well defined convergence with a fluctuation of about 10^{-5}. In Fig. 2.1.12 the same applies. We can then conclude that a choice of $n_{max} = 80$ are sufficient for the given values of l_0/a_0 and l. For two dimension one should expect to see the same results. In Fig. 2.1.13 and 2.1.14 the same ϵ are plotted as a function of n_{max}. We clearly see the same behavior as in three dimensions. Note how much more severe the convergence for $l_0/a_0 = 1$ are in two dimensions. At $n_{max} = 80$ we have one magnitude difference in ϵ. For two dimensions we conclude that $n_{max} = 80$ are sufficient except for $l_0/a_0 = 1$, where we should increase n_{max} to 100.

2.2 Perturbation as an alternative

Until now we have discussed what numerical schemes we should use for the calculations but we have left out any analytical approximation. The most known are probably perturbation theory. Its has a wide range of application and it would be interesting to investigate how it handles our problem. To second order we have

$$E_n = E_n^0 + \langle n^0|H_1|n^0\rangle + \sum_{n'\neq n} \frac{|\langle n'|H_1|n^0\rangle|^2}{E_n^0 - E_{n'}^0}. \tag{2.108}$$

See App. A.4 for the derivation of second order perturbation theory. A necessary condition for perturbation is that the perturbation term is small compared to

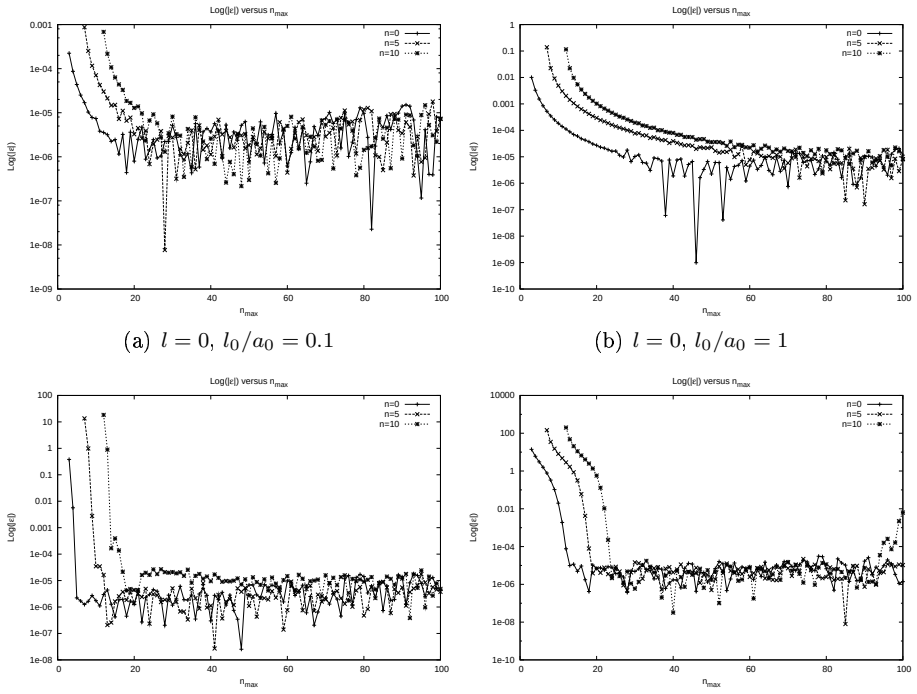

(a) $l = 0$, $l_0/a_0 = 0.1$ (b) $l = 0$, $l_0/a_0 = 1$

(c) $l = 0$, $l_0/a_0 = 10$ (d) $l = 0$, $l_0/a_0 = 100$

Figure 2.1.11: Relative error as a function of matrix cutoff n_{max} for three dimensions and $l = 0$.

the calculable exact term. In our case we would threat the Coulomb interaction as a perturbation and the single particle Hamiltonians as the calculable terms. The Coulomb interaction goes as $1/r$ and as long as r is sufficiently big, this term is small. In our case the oscillator length l_0 will also determine the strength of the interaction. To calculate the integrals in the perturbation expansion we still use Gauss-Laguerre techniques. The series in Eq. (2.108) need to be terminated at some n_max' and for comparison reasons we terminate this at n_max. By doing this, we ensure that we include the same number of corrections in both the perturbation expansion and the matrix diagonalization. In Fig. **??** and **??** we have plotted the a relative error $|\epsilon|$ as a function of l_0/a_0 for two and three dimensions respectively. The relative error are taken as the ratio between the matrix diagonalization and second order perturbation theory minus one. Both the matrix and perturbation series are terminated at $n_max' = n_max = 80$ for both two and three dimensions. Note however that we should increase the cut-off to 100 for $l_0/a_0 = 1$ in the two dimensional case as commented earlier. This have not been done here, as we are interested in the total picture rather than the specific case of $l_0/a_0 = 1$. The condition in Eq. (A.107) is clearly illustrated for both two and three dimensions. For the lowest eigenvalues we need to go as low as $l_0/a_0 = 0.01$ to get a relative error of 10^{-5} which still is quite high. In addition remember that both these methods are approximates to a solution we do not know exactly. Hence it is hard to recommend or disregard perturbation theory. However, one thing is for sure, it is much more limited

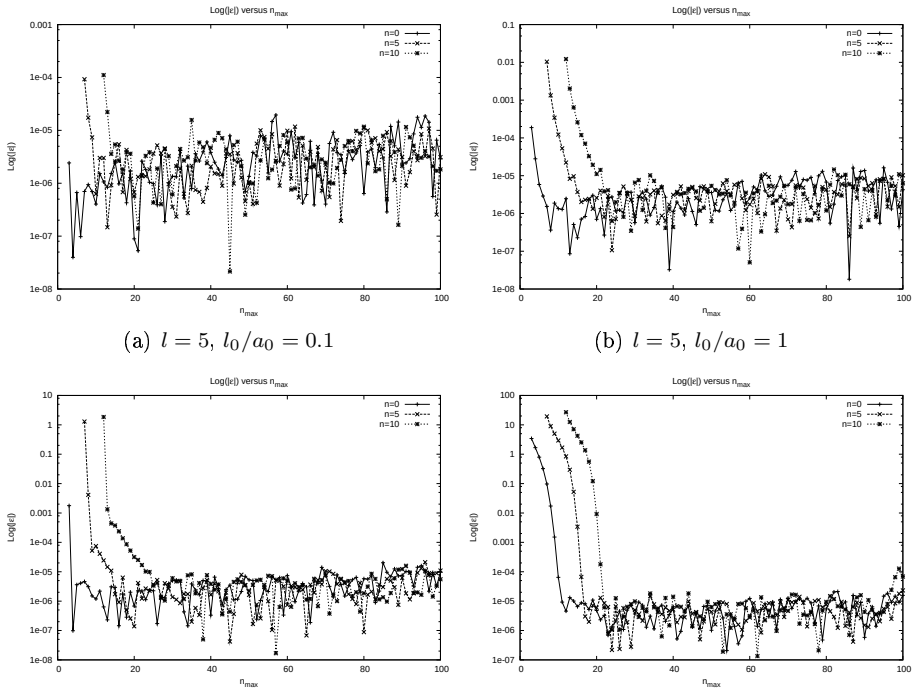

(a) $l = 5$, $l_0/a_0 = 0.1$ (b) $l = 5$, $l_0/a_0 = 1$

(c) $l = 5$, $l_0/a_0 = 10$ (d) $l = 5$, $l_0/a_0 = 100$

Figure 2.1.12: Relative error as a function of matrix cutoff n_{max} for three dimensions and $l = 5$.

than matrix diagonalization techniques regarding the choice of l_0/a_0. Thus, we will not be using perturbation in this thesis. But its results will be compared with the matrix diagonalization for small values of l_0/a_0. But it could be a viable options for Coulomb problems where l_0/a_0 is sufficiently low since it is more computer efficient and do not include any diagonlization algorithms.

2.3 Diagonalization results

The techniques we employ have now been determined and it is time to put them to good use. Eigenvalues obtained by diagonalization for two dimensions are listed in Tab. 2.3.5-2.3.8 for different values of m and l_0/a_0. While Tab. 2.3.9-2.3.12 lists the results for three dimensions. In Sec. 1.4.1 and 1.4.2 we plotted Fock-Darwin spectra of the eigenvalues. For comparison reasons it would be preferable to develop the same kind of spectra in this section. However, due to the interacting Coulomb potential we have no way of plotting Fock-Darwin spectra without handling units properly. For a two dimensional, non-interacting dot Eq. (1.28) gives the energy as

$$\frac{E}{\hbar\omega_0} = (2n + |m| + 1)\sqrt{1 + \frac{\omega_B^2}{\omega_0^2}} + m\frac{\omega_B}{\omega_0}. \tag{2.109}$$

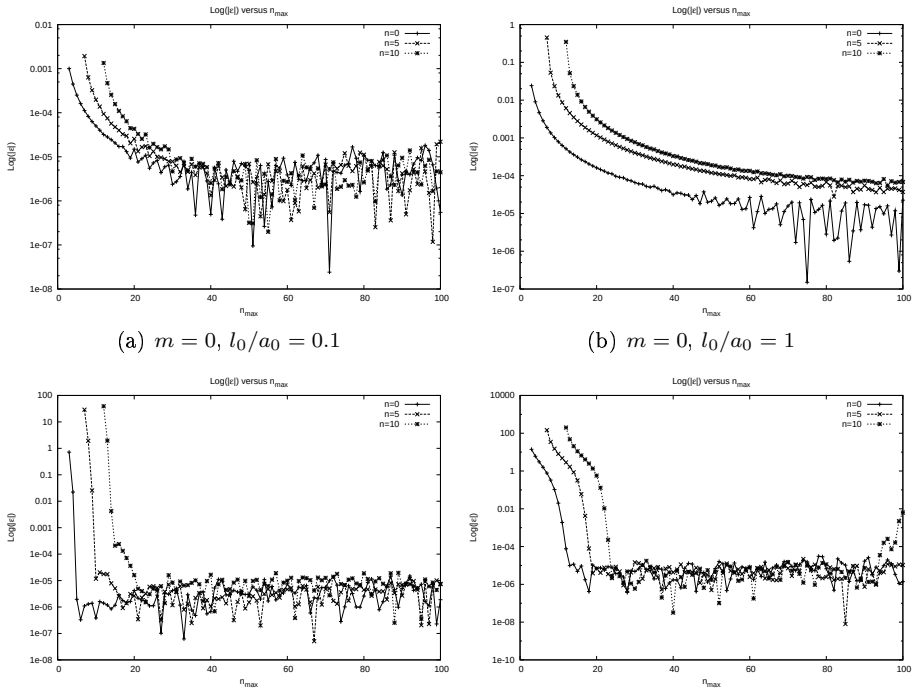

(a) $m = 0$, $l_0/a_0 = 0.1$ (b) $m = 0$, $l_0/a_0 = 1$

(c) $m = 0$, $l_0/a_0 = 10$ (d) $m = 0$, $l_0/a_0 = 100$

Figure 2.1.13: Relative error as a function of matrix cutoff n_{max} for two dimensions and $m = 0$.

l_0/a_0	0			
m	0		5	
n	$E/\hbar\omega$	$E'/\hbar\omega$	$E/\hbar\omega$	$E'/\hbar\omega$
0	2.000000	2.000000	7.000000	7.000000
1	4.000000	4.000000	9.000000	9.000000
2	6.000000	6.000000	11.000000	11.000000
3	8.000000	8.000000	13.000000	13.000000
4	10.000000	10.000000	15.000000	15.000000
5	12.000000	12.000000	17.000000	17.000000
6	14.000000	14.000000	19.000000	19.000000
7	16.000000	16.000000	21.000000	21.000000
8	18.000000	18.000000	23.000000	23.000000
9	20.000000	20.000000	25.000000	25.000000
10	22.000000	22.000000	27.000000	27.000000

Table 2.3.5: Lowest eigenvalues in two dimensions for $m = 0, 5$ and $l_0/a_0 = 0$.

Adding the correction term in two dimension from Eq. (2.88) we get

$$\frac{\epsilon_r}{\hbar\omega_0} = (2n + |m| + 1)\sqrt{1 + \frac{\omega_B^2}{\omega_0^2}} + m\frac{\omega_B}{\omega_0} + \frac{l_0}{4a_0}\frac{\omega}{\omega_0}I_{2D}. \tag{2.110}$$

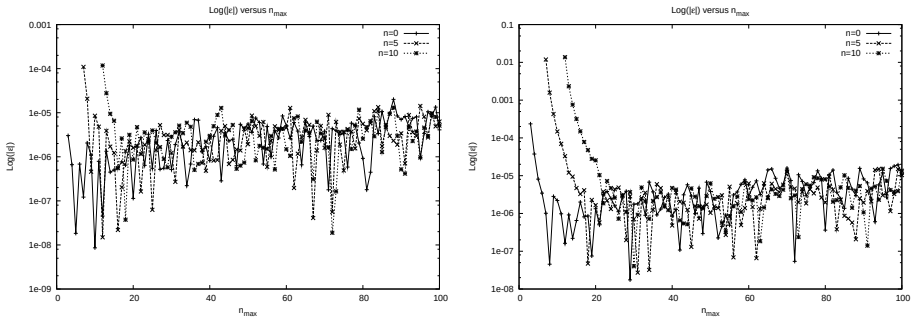

(a) $m = 5$, $l_0/a_0 = 0.1$ (b) $m = 5$, $l_0/a_0 = 1$

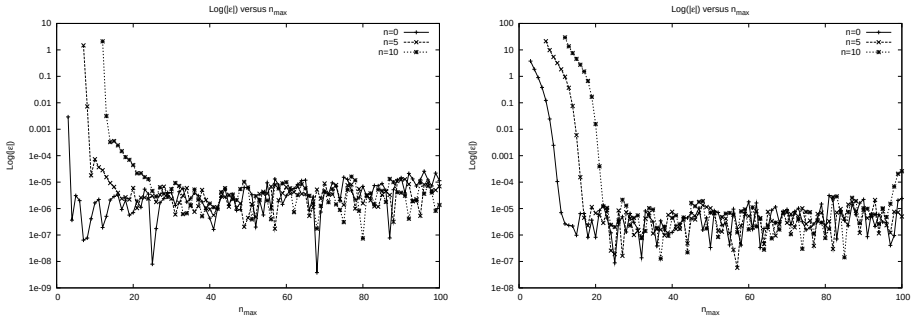

(c) $m = 5$, $l_0/a_0 = 10$ (d) $m = 5$, $l_0/a_0 = 100$

Figure 2.1.14: Relative error as a function of matrix cutoff n_{max} for two dimensions and $m = 5$.

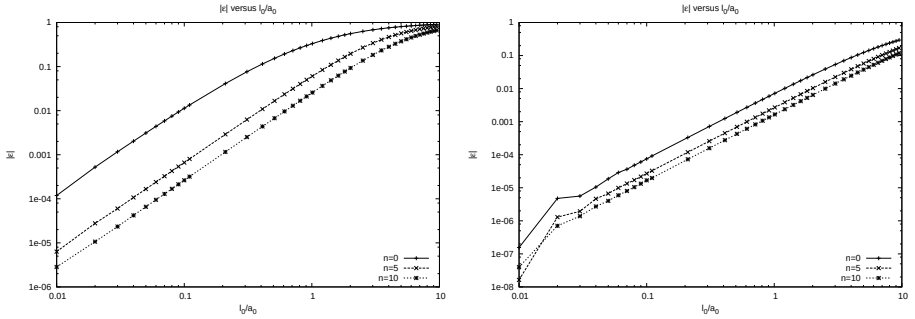

(a) $m = 0$ (b) $m = 5$

Figure 2.2.15: Relative error between matrix diagonalization and second order perturbation theory in two dimensions.

The matrix I_{2D}'s elements are defined in Eq. (2.94). Since l_0 depends on ω we need to collect the constant factors in front of the matrix into one expression. By writing

$$\frac{l_0}{a_0^*}\frac{\omega}{\omega_0} = \frac{e^2 m}{4\pi\epsilon\epsilon_0\hbar^2}\sqrt{\frac{\hbar}{m\omega}}\sqrt{\frac{\omega}{\omega_0}}, \tag{2.111}$$

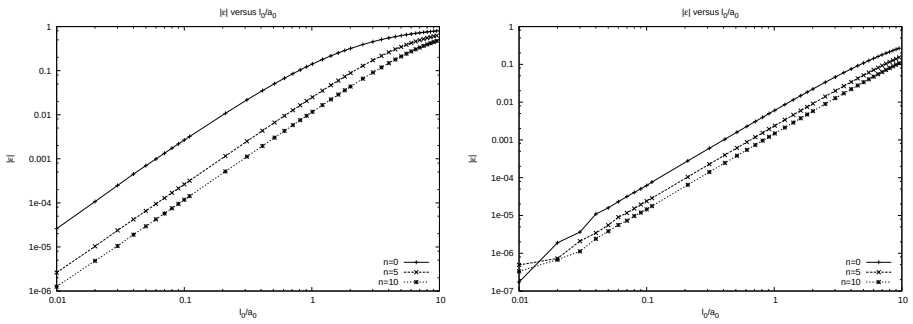

(a) $m = 0$ (b) $m = 5$

Figure 2.2.16: Relative error between matrix diagonalization and second order perturbation theory in three dimensions.

l_0/a_0	0.01			
m	0		5	
n	$E/\hbar\omega$	$E'/\hbar\omega$	$E/\hbar\omega$	$E'/\hbar\omega$
0	2.017672	2.017793	7.004365	7.004366
1	4.013282	4.013389	9.004186	9.004184
2	6.011348	6.011445	11.004031	11.004032
3	8.010181	8.010261	13.003897	13.003901
4	10.009355	10.009434	15.003782	15.003786
5	12.008740	12.008809	17.003685	17.003685
6	14.008243	14.008314	19.003592	19.003595
7	16.007844	16.007908	21.003509	21.003513
8	18.007508	18.007566	23.003434	23.003438
9	20.007219	20.007272	25.003365	25.003370
10	22.006957	22.007016	27.003306	27.003307

Table 2.3.6: Lowest eigenvalues in two dimensions for $m = 0, 5$ and $l_0/a_0 = 0.01$.

then rearrange and multiply the speed of light in the denominator and nominator we get

$$\frac{l_0}{a_0^*}\frac{\omega}{\omega_0} = \frac{e^2}{4\pi\epsilon\epsilon_0\sqrt{\hbar\omega_0}}\sqrt{\frac{mc^2}{\hbar^2c^2}}\sqrt{\frac{\omega}{\omega_0}}. \tag{2.112}$$

If we now set our energy scale by letting $\hbar\omega_0 = 1eV$ and substitute the known values for mc^2 and $\hbar^2c^2$ from [12] into the equation above we get

$$\frac{l_0}{a_0^*}\frac{\omega}{\omega_0} \approx 5.325\gamma\sqrt{\frac{\omega}{\omega_0}}. \tag{2.113}$$

Where γ handles the correction from ϵ and the reduced mass difference. If we put $\gamma = 1$ our system will be in vacuum with reduced electron mass equal to the bare electron mass. Let us substitute Eq. (2.113) into Eq. (2.110) and using

l_0/a_0	0.1		1	
m	0		5	
n	$E/\hbar\omega$	$E/\hbar\omega$	$E/\hbar\omega$	$E/\hbar\omega$
0	2.170701	7.043581	3.320181	7.431919
1	4.131206	9.041765	5.148608	9.414608
2	6.112746	11.040245	7.035210	11.399959
3	8.101315	13.038939	8.953420	13.387311
4	10.093282	15.037806	10.890837	15.376212
5	12.087186	17.036794	12.840876	17.366357
6	14.082335	19.035886	14.799742	19.357513
7	16.078354	21.035068	16.765071	21.349493
8	18.074989	23.034319	18.735281	23.342178
9	20.072110	25.033643	20.709321	25.335455
10	22.069591	27.033006	22.686416	27.329250

Table 2.3.7: Lowest eigenvalues in two dimensions for $m = 0, 5$ and $l_0/a_0 = 0.1, 1$. Perturbation are not available due to non-accepting accuracy.

l_0/a_0	10		100	
m	0		5	
n	$E/\hbar\omega$	$E/\hbar\omega$	$E/\hbar\omega$	$E/\hbar\omega$
0	8.821806	10.995593	34.181240	34.758886
1	10.585394	12.877493	35.920815	36.512759
2	12.375899	14.772193	37.667653	38.273712
3	14.188776	16.677455	39.421444	40.041442
4	16.020389	18.591561	41.181908	41.815668
5	17.867843	20.513186	42.948790	43.596107
6	19.728798	22.441228	44.721802	45.382512
7	21.601359	24.374829	46.500719	47.174621
8	23.483983	26.313275	48.285293	48.972223
9	25.375390	28.255971	50.075292	50.775079
10	27.274505	30.202437	51.870515	52.582985

Table 2.3.8: Lowest eigenvalues in two dimensions for $m = 0, 5$ and $l_0/a_0 = 10, 100$. Perturbation are not available due to non-accepting accuracy.

the definitions of ω, ω_B and ω_0 from Ap. A.6.1 we get

$$\epsilon_r^{2D} \approx (2n + |m| + 1)\sqrt{1 + \frac{\omega_B^2}{\omega_0^2}} + m\frac{\omega_B}{\omega_0} + \frac{5.325\gamma}{4} I_{2D} \left(1 + \frac{\omega_B^2}{\omega_0^2}\right)^{1/4}. \quad (2.114)$$

The same expression can easily be developed for three dimensions by adding the interacting correction to Eq. (1.47). This gives

$$\epsilon_r^{3D} \approx \left(2n + l + \frac{3}{2}\right)\sqrt{1 + \frac{\omega_B^2}{\omega_0^2}} + m\frac{\omega_B}{\omega_0} + \frac{5.325\gamma}{4} I_{3D} \left(1 + \frac{\omega_B^2}{\omega_0^2}\right)^{1/4}. \quad (2.115)$$

l_0/a_0	0			
m	0		5	
n	$E/\hbar\omega$	$E'/\hbar\omega$	$E/\hbar\omega$	$E'/\hbar\omega$
0	3.000000	3.000000	8.000000	8.000000
1	5.000000	5.000000	10.000000	10.000000
2	7.000000	7.000000	12.000000	12.000000
3	9.000000	9.000000	14.000000	14.000000
4	11.000000	11.000000	16.000000	16.000000
5	13.000000	13.000000	18.000000	18.000000
6	15.000000	15.000000	20.000000	20.000000
7	17.000000	17.000000	22.000000	22.000000
8	19.000000	19.000000	24.000000	24.000000
9	21.000000	21.000000	26.000000	26.000000
10	23.000000	23.000000	28.000000	28.000000

Table 2.3.9: Lowest eigenvalues in three dimensions for $l = 0, 5$ and $l_0/a_0 = 0$.

l_0/a_0	0.01			
m	0		5	
n	$E/\hbar\omega$	$E'/\hbar\omega$	$E/\hbar\omega$	$E'/\hbar\omega$
0	3.011267	3.011312	8.004171	8.004172
1	5.009408	5.009435	10.004008	10.004012
2	7.008362	7.008401	12.003872	12.003875
3	9.007674	9.007708	14.003753	14.003757
4	11.007165	11.007197	16.003652	16.003653
5	13.006775	13.006797	18.003553	18.003561
6	15.006441	15.006471	20.003473	20.003477
7	17.006174	17.006198	22.003399	22.003402
8	19.005941	19.005965	24.003325	24.003333
9	21.005740	21.005762	26.003261	26.003269
10	23.005558	23.005582	28.003201	28.003210

Table 2.3.10: Lowest eigenvalues in three dimensions for $l = 0, 5$ and $l_0/a_0 = 0.01$.

The matrix elements of I_{3D} and I_{2D} are defined in Eq. (2.96) and 2.94 respectively. By using the same matrix diagonalization as before we can evaluate ϵ_r in both two and three dimension and plot them to form Fock-Darwin spectra. The results can then be compared with the non-interacting case in Sec. 1.4.1. Four two-dimensional Fock-Darwin spectrum in are plotted in Fig. 2.3.17. One for each value of γ. We clearly see the exact same behavior as Fig. 1.4.6 for $\gamma = 0$. This is expected since $\gamma = 0$ turn of the interaction. When we increase γ we see the breaking of the Landau levels. The dotted lines are the limits when the magnetic field goes to infinity. For $\gamma = 0.1$ only the lowest levels seem to break, but for $\gamma = 10$ we have a complete breakdown. Without the interaction the particles have no problem resting in the Landau levels as the magnetic field increase. By adding the interaction one have repulsion between the particles and if we try to push them into specific Landau levels, their energy increase as

l_0/a_0	0.1		1	
m	0		5	
n	$E/\hbar\omega$	$E/\hbar\omega$	$E/\hbar\omega$	$E/\hbar\omega$
0	3.111312	8.041656	4.000038	8.413250
1	5.093421	10.040052	5.880322	10.397889
2	7.083337	12.038698	7.801196	12.384757
3	9.076552	14.037530	9.743691	14.373306
4	11.071513	16.036482	11.699278	16.363187
5	13.067559	18.035553	13.663510	18.354152
6	15.064336	20.034725	15.633831	20.345986
7	17.061634	22.033968	17.608627	22.338577
8	19.059322	24.033280	19.586842	24.331785
9	21.057315	26.032643	21.567744	26.325523
10	23.055530	28.032061	23.550788	28.319736

Table 2.3.11: Lowest eigenvalues in three dimensions for $l = 0, 5$ and $l_0/a_0 = 0.1, 1$. Perturbation are not available due to non-accepting accuracy.

l_0/a_0	10		100	
m	0		5	
n	$E/\hbar\omega$	$E/\hbar\omega$	$E/\hbar\omega$	$E/\hbar\omega$
0	9.350610	11.855797	34.687119	35.377642
1	11.117484	13.746849	36.426850	37.134252
2	12.911140	15.649341	38.173834	38.897900
3	14.727020	17.561329	39.927787	40.668284
4	16.561527	19.481307	41.688408	42.445121
5	18.411763	21.408077	43.455427	44.228109
6	20.275391	23.340689	45.228587	46.017031
7	22.150540	25.278381	47.007646	47.811620
8	24.035661	27.220488	48.792359	49.611651
9	25.929483	29.166513	50.582516	51.416898
10	27.830936	31.115991	52.377881	53.227148

Table 2.3.12: Lowest eigenvalues in three dimensions for $l = 0, 5$ and $l_0/a_0 = 10, 100$. Perturbation are not available due to non-accepting accuracy.

they get closer to each other. If the interaction is weak, for example if we have a very small reduced electron mass we would be able to push the particles closer together almost forming Landau levels. The reason why the lowest levels break down first is because of confinement. For the lowest lying states, the particles are closer bound due to the orbitals determined by m. Hence, the interaction are stronger and we get breakdown at the lowest lying states before the higher ones become apparent. By increasing the magnetic field, the breakdown of the higher levels will be unveiled. The same can be observed in Fig. 2.3.18 which plots three dimensional Fock-Darwin spectrum for the same γ values as for two dimensions. Observe how much more complicated the spectrum is for $\gamma = 1, 10$. This is due to the added degeneracy. Up until now we have developed complete

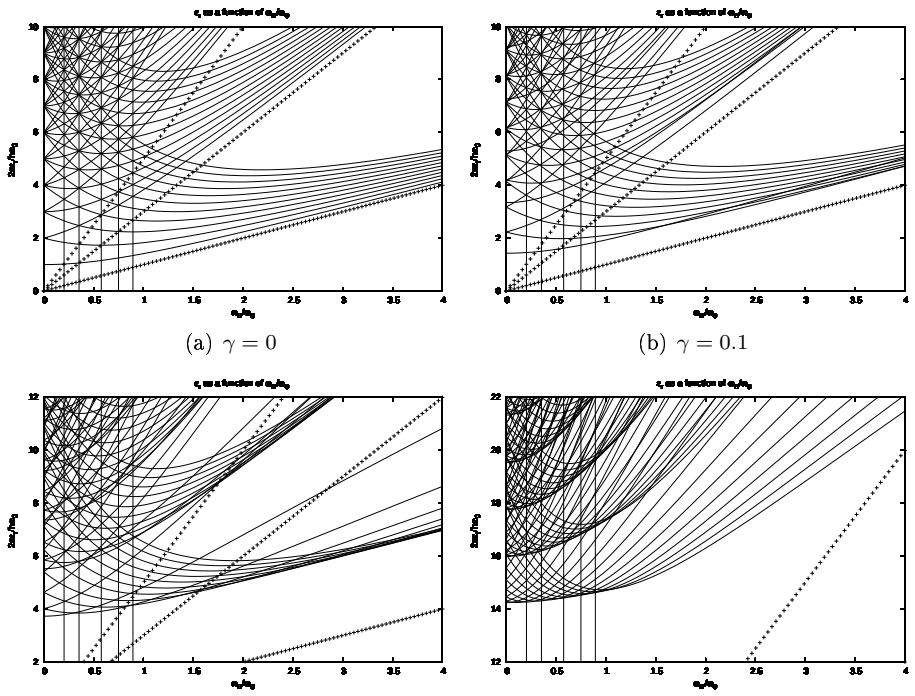

(a) $\gamma = 0$ (b) $\gamma = 0.1$

(c) $\gamma = 1$ (d) $\gamma = 10$

Figure 2.3.17: Fock-Darwin spectrum in two dimensions for different values of γ.

comparison between two and three dimensional harmonic oscillators. First we looked at the single particle harmonic oscillators and then added the interaction term in the relative part. This gave us a complete different Fock-Darwin spectrum, especially for strong interactions. What we now want to do is look ahead and investigate several particles in a harmonic oscillator confinement. The structure need to be investigated as practical quantum dots would probably contain more than two isolated electrons. It would be reasonable to believe that the structure complexity would increase with the electron number. It also gives us more depth knowledge about the artificial atoms with higher electron number than two.

3 Structure of quantum dots with more than two electrons

The center-of-mass and relative separation we employed in the last sections is an excellent way of treating two particles. However when we want to include more particles we run into problems. We have no logical way of describing several particles in the center-of-mass notation, unless we include a modified center of mass and relative motion between each particle. The center-of-mass term would be very complicated as the particle number increase. Hence we cannot use this basis anymore. We need to transform from center-of-mass coordinates to what

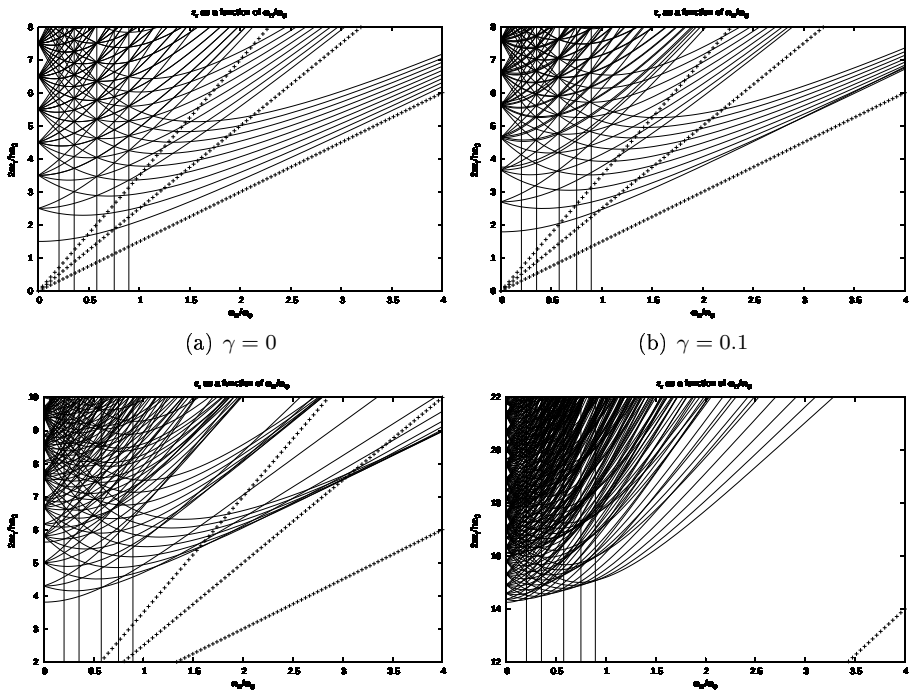

(a) $\gamma = 0$ (b) $\gamma = 0.1$

(c) $\gamma = 1$ (d) $\gamma = 10$

Figure 2.3.18: Fock-Darwin spectrum in three dimensions for different values of γ.

we will refer to as laboratory coordinates. Laboratory coordinates are just the polar coordinate system with a labeling of the quantum number which reflect single particles. This will be clearer as we start to work on the transformations.

3.1 Transformation from center-of-mass to laboratory basis

In this section we will develop a transformation from the center-of-mass basis to the laboratory basis in both two and three dimensions. We will follow much of the work done in [5]. As this is a central part of the thesis, calculations are given in details where needed. The harmonic oscillator basis is of interest to us, and it is this basis we are going to transform. As in the last section we will use Dirac notation due to its simplicity. The total angular momentum from Eq. (1.59) do commute with both the Hamiltonian in Eq. (1.11) and its three dimensional counterpart. The total angular momentum will now be referred to as L_{tot}. This means that we can construct eigenfunctions of L_T^2,L_{T_z} and H. This should not come as a surprise as we did this in Sec. 1.4. As elsewhere in this thesis we will label the center-of-mass quantum numbers and coordinates by capitol letters, while we use small letters on the relative analogy. Using Dirac notation we can

write out the eigenstates in the three dimensional center-of-mass basis as

$$|nl, NL, L_T M_T\rangle = \sum_{mM} \langle lLmM|L_T M_T\rangle \psi_{nl}(r)\Omega_{lm}(\theta,\phi)\psi_{NL}(R)\Omega_{LM}(\Theta,\Phi). \tag{3.116}$$

Doing just the same for the laboratory basis gives

$$\begin{aligned} |n_1 l_1, n_2 l_2, \tilde{L}_T \tilde{M}_T\rangle &= \sum_{m_1 m_2} \langle l_1 l_2 m_1 m_2|\tilde{L}_T \tilde{M}_T\rangle \psi_{n_1 l_1}(r_1)\Omega_{l_1 m_1}(\theta_1,\phi_1) \\ &\times \psi_{n_2 l_2}(r_2)\Omega_{l_2 m_2}(\theta_2,\phi_2). \end{aligned} \tag{3.117}$$

Where $\langle lLmM|L_T M_T\rangle$ and $\langle l_1 l_2 m_1 m_2|L_T M_T\rangle$ are the respective Clebsch-Gordon coefficients. See [19] for details. Since the total angular momenta is conserved, $\tilde{L}_T = L_T$ and $\tilde{M}_T = M_T$. We want to find a transformation between $|nl, NL, L_T M_T\rangle$ and $|n_1 l_1, n_2 l_2, L_T M_T\rangle$. By using the completeness relation we can write the transformation as

$$|n_1 l_1, n_2 l_2, L_T M_T\rangle = \sum_{nlNL} |nl, NL, L_T M_T\rangle\langle nl, NL, L_T M_T|n_1 l_1, n_2 l_2, L_T M_T\rangle. \tag{3.118}$$

From [20] we know that the bracket in Eq. (3.118) is independent of M_T. Hence it is dropped from the bracket in further calculation. When doing the transformation the energy needs to be conserved. Comparing the solutions of Eq. (1.74) and the three dimensional counterpart of Eq. (1.11) we get the relation

$$2n_1 + l_1 + 2n_2 + l_2 = 2n' + l' + 2N' + L'. \tag{3.119}$$

Where we have redefined $n' = 2n$, $l' = 2l$, $N' = 2N$ and $L' = L/2$. This makes the sum in Eq. (3.118) finite due to the restriction posed by Eq. (3.119) and nonzero by the triangle inequality

$$|l_1 - l_2| \leq L_T \leq l_1 + l_2, \tag{3.120}$$

and

$$m_1 + m_2 = M_T. \tag{3.121}$$

The two last equation are properties of the Clebsh-Gordon coefficients. (FINN REF). As we are investigating the Coulomb interaction we will now observe what will happen with the matrix elements during the transformation. Instead of illustrating this using the Coulomb interaction, we use the general interaction $V(r)$. Using Eq. (3.118) the matrix elements of this interaction could be written as

$$\begin{aligned} &\langle n_1 l_1, n_2 l_2, L_T M_T|V(r)|n_1' l_1', n_2' l_2', L_T' M_T'\rangle = \\ &\sum_{nlNL}\sum_{n'l'N'L'} \langle n_1 l_1, n_2 l_2, L_T|nl, NL, L_T\rangle \times \\ &\qquad \langle n'l', N'L', L_T'|n_1' l_1', n_2' l_2', L_T'\rangle \times \\ &\qquad\qquad \langle nl, NL, L_T M_T|V(r)|n'l', N'L', L_T' M_T'\rangle. \end{aligned} \tag{3.122}$$

The interaction only depends on the relative coordinates the last bracket in Eq. (3.122) simplifies to

$$\langle nl, NL, L_T M_T | V(r) | n'l', N'L', L'_T M'_T \rangle = \langle nl | V(r) | n'l' \rangle \delta_{NN'} \delta_{ll'} \delta_{LL'} \delta_{L_T L'_T} \delta_{M_T M'_T}. \tag{3.123}$$

This bracket could be evaluated explicitly using the series expansion over the Talmi integrals. See Sec. 2.1 for details. Substitute Eq. (3.123) into Eq. (3.122) gives

$$\langle n_1 l_1, n_2 l_2, L_T M_T | V(r) | n'_1 l'_1, n'_2 l'_2, L_T M_T \rangle = \sum_{nlNL} \langle nl, NL, L_T | n_1 l_1, n_2 l_2, L_T \rangle \langle n'l, NL, L_T | n'_1 l'_1, n'_2 l'_2, L_T \rangle \langle nl | V(r) | n'l \rangle. \tag{3.124}$$

If we now could find an expression for the two unknown brackets in the sum we could calculate both the transformations and the integral explicitly using Talmi integrals. However, for reason explained in Sec. 2.1 we will not be using series expansion of the interacting part. But the transformation as of great importance to us. First we will develop a recurrence relation between successive quantum numbers. Let us first consider $|(n_1+1)l_1, n_2 l_2, L_T M_T\rangle$. Using the recurrence relation for the Laguerre polynomials in (SKRIV NED REC. FORMEL I SEC 6.1) and the eigenfunction in Eq. (A.184),substituting $\rho_1^2 = \beta r_1^2$ and remember that the spherical angle dependent eigenfunctions are independent on change of n_1, we obtain

$$|(n_1+1)l_1, n_2 l_2, L_T M_T\rangle = \sqrt{\frac{2(n_1+1)!}{(n_1+l_1+3/2)!}} \rho^{l_1} e^{-\rho_1^2/2} \times \Sigma(\rho_2, \theta_1, \theta_2, \phi_1, \phi_2) L_{n_1+1}^{l_1+1/2}(\rho^2). \tag{3.125}$$

Where we have collected radial eigenfunction for the second particle and both angle dependent eigenfunction in one term called Σ. Substituting the recurrence relation gives

$$|(n_1+1)l_1, n_2 l_2, L_T M_T\rangle = \sqrt{\frac{2(n_1+1)!}{(n_1+l_1+3/2)!}} \rho_1^l e^{\rho_1^2/2} \Sigma(\rho_2, \theta_1, \theta_2, \phi_1, \phi_2) \times \left\{ \frac{2n_1 + l_1 + 3/2 - \rho_1^2}{n_1+1} L_n^{l_1+1/2}(\rho_1^2) - \frac{(n_1+l_1+1/2)}{n_1+1} L_{n-1}^{l_1+1/2}(\rho_1^2) \right\}, \tag{3.126}$$

using the factorial relation $(n+1)! = (n+1)n!$ we can simplify the equation as

$$|(n_1+1)l_1, n_2l_2, L_TM_T\rangle = \left(2n_1 + l_1 + \frac{3}{2}\right)\sqrt{\frac{1}{(n_1+1)(n_1+l_1+3/2}}|n_1l_1, n_2l_2, L_TM_T\rangle - \sqrt{\frac{n_1(n_1+l_1+1/2)}{(n_1+1)(n_1+l_1+3/2)}}|(n_1-1)l_1, n_2l_2, L_TM_T\rangle. \tag{3.127}$$

If we multiplying from left with $\langle nl, NL, L_TM_T|$, the left hand side will be zero unless

$$2n_1 + l_1 + 2n_2 + l_2 + 2 = 2n + l + 2N + L. \tag{3.128}$$

This can be observed from Eq. (3.119). For the same reason we have limitations on the right hand brackets. When the left hand side are non-zero by Eq. (3.128) the right hand brackets will be zero. This leaves us with an equation as

$$\langle nl, NL, L_TM_T|(n_1+1)l_1, n_2l_2, L_TM_T\rangle = -\sqrt{\frac{1}{(n_1+1)(n_1+l_1+3/2)}} \times \langle nl, NL, L_TM_T|\rho_1^2|n_1l_1, n_2l_2, L_TM_T\rangle, \tag{3.129}$$

using the completeness relation gives

$$\langle nl, NL, L_TM_T|(n_1+1)l_1, n_2l_2, L_TM_T\rangle = -\sqrt{\frac{1}{(n_1+1)(n_1+l_1+3/2)}} \times \sum_{\tilde{n}\tilde{l}\tilde{N}\tilde{L}} \langle nl, NL, L_TM_T|\rho_1^2|\tilde{n}\tilde{l}, \tilde{N}\tilde{L}, L_TM_T\rangle \times \langle \tilde{n}\tilde{l}, \tilde{N}\tilde{L}, L_T|n_1l_1, n_2l_2, L_T\rangle. \tag{3.130}$$

Observe the recursion form of Eq. (3.129). Again we see that we only get contributions when

$$2n + l + 2N + L = 2\tilde{n}_1 + \tilde{l}_1 + 2\tilde{n}_2 + \tilde{l}_2 + 2. \tag{3.131}$$

If we now had a way to calculate the matrix elements in Eq. (3.130) we could determine all transformation brackets in Eq. (3.118) and hence have a proper transformation which is easily implemented on a computer. The matrix elements can be calculated in several ways and is not shown explicitly in this section as it is done elsewhere. See for example Sec. 2.1 where the analogy should be clear. To be able to calculate the elements one need to transform r_1 into a r and R dependent expression. Using Eq. (1.50) and 1.51 we can express r_1 in relative and center-of-mass coordinates so they relate to the bra and kets. Recursion relation starts somewhere and in our case it would be natural to start at $\langle nl, NL, L_T|0l_1, 0l_2, L_T\rangle$. Up until now we have no clue how l and L transforms. Thus we will now develop an explicit expression for this bracket. This notation also suits us well, as we diagonalize for each l and L. We only

need to calculate this bracket once in the diagonalization process. It turns out that $\langle nl, NL, L_T|0l_1, 0l_2, L_T\rangle$ involves quite large factorial ratios, which increase computing time while decreasing accuracy.

3.2 Matrix reduction using Lee-Suzuki effective interactions

A Appendix

A.1 Lanczos methods

In the this section we will develop a method that is an alternative to the Householder method used elsewhere in this thesis. An optimal way of finding eigenvalues and eigenvector is first to reduce the matrix to a simple form, often triangular and then start the iterative process. The Householder method is one of the most effective methods of reducing the matrix. A $n \times n$ matrix is reduced to tridiagonal form by $n-2$ orthogonal transformations (FINN REF). See [14] for details. The operations needed goes as $2n^3/4$. As the matrices becomes large, we will get performance issues with this method. In addition, the Householder reduction may give roundoff errors when the matrix elements vary over many orders of magnitude. If our matrix is sparse, the orthogonal transformation destroys the sparsity. As a result we get larger dense matrices during the reduction. However, in many cases only the extreme eigenvalues are of interest. Doing complete matrix diagonalization is simply not needed. The Lanczos algorithm is one of the most effective computational tools for searching few extreme eigenvalues and corresponding eigenvectors. The application in physics and mathematics are countless. In this section we will give a brief introduction to the Lanczos algorithm. At the end we will discuss convergence and its downsides. Let us first assume that we have a large, sparse and symmetric matrix $A \in \Re^{n\times n}$ in the eigenproblem $Ax = \lambda x$. Then assume that only the extreme eigenvalues are of interest to us. Also note that symmetric matrices can be expressed as $A = QDA^T$, where Q is an orthogonal matrix and D is a diagonal matrix containing the eigenvalues. Looking at the Rayleigh quotient

$$r(x) = \frac{\vec{x}^T A\vec{x}}{\vec{x}^T\vec{x}} \quad \vec{x} \neq 0, \tag{A.1}$$

we observe that the maximum and minimum values of $r(x)$ would be the eigenvalues $\lambda_1(A)$ and $\lambda_m(A)$ respectively. Now suppose $Q_i = [q_1, ..., q_i]$ is orthogonal. Define scalars M_i and m_i as

$$M_i = \lambda_1(Q_i^T A Q_i), \tag{A.2}$$
$$m_i = \lambda_i(Q_i^T A Q_i). \tag{A.3}$$

A new Rayleigh quotient is defined with eigenvector y to give

$$M_i = \max_{\vec{y}\neq 0} \frac{\vec{y}^T(Q_i^T A Q_i)\vec{y}}{\vec{y}^T\vec{y}}, \tag{A.4}$$
$$m_i = \min_{\vec{y}\neq 0} \frac{\vec{y}^T(Q_i^T A Q_i)\vec{y}}{\vec{y}^T\vec{y}}. \tag{A.5}$$

Comparing this with Eq. (A.1) would yield the following relations

$$M_i = \max_{\|\vec{y}\|_2=1} r(Q_i\vec{y}) \leq \lambda_1(A), \tag{A.6}$$
$$m_i = \max_{\|\vec{y}\|_2=1} r(Q_i\vec{y}) \geq \lambda_m(A), \tag{A.7}$$

where

$$\|\vec{y}\|_2 = \vec{y}^T\vec{y}. \tag{A.8}$$

The main purpose of the Lanczos algorithm is to generate the q_i in such way that M_i and m_i gets increasingly closer to λ_1 and λ_m. The gradient of the Rayleigh quotient need to be calculated. First we explicitly write out the Rayleigh quotient

$$r(x) = \frac{\sum_{j=1}^{n}\sum_{k=1}^{n} A_{jk}x_jx_k}{\sum_{j=1}^{n} x_j^2}, \tag{A.9}$$

where n is the number of components in $\vec{x}$. Taking the derivative with respect to x_q we get the expression

$$\frac{\partial r(x)}{\partial x_q} = \sum_{j=1}^{n}\sum_{k=1}^{n} A_{jk}x_jx_k\frac{\partial}{\partial x_q}\left(\frac{1}{\sum_{j=1}^{n} x_j^2}\right) + \frac{1}{\sum_{j=1}^{n} x_j^2}\frac{\partial}{\partial x_q}\left(\sum_{j=1}^{n}\sum_{k=1}^{n} A_{jk}x_jx_k\right), \tag{A.10}$$

expanding and performing the derivatives yields

$$\frac{\partial r(x)}{\partial x_q} = -2\sum_{q}\sum_{k} A_{qk}x_qx_k\frac{1}{\sum_q x_q^3} + \frac{1}{\sum_j x_j^2}\left(\sum_k A_{qk}x_k + \sum_j A_{jq}x_j\right). \tag{A.11}$$

Because of the symmetry of A we combine the two last sums into one and the Rayleigh gradient can now be written as

$$\nabla r(x) = \frac{2}{\vec{x}^T\vec{x}}\left(A\vec{x} - r(x)\vec{x}\right). \tag{A.12}$$

Suppose $u_k \in \text{span}\{q_1, ..., q_{i+1}\}$ is such that $M_k = r(u_k)$. We want to make sure $M_{i+1} > M_i$. This can be done by demanding that

$$\nabla r(u_i) \in \text{span}\{q_1, ..., q_{i+1}\}, \tag{A.13}$$

from where q_{i+1} can be determined. This can be ensured since $r(x)$ increase most rapidly in the direction of the its gradient. If $v_i \in \text{span}\{q_1, ..., q_{i+1}\}$ satisfies $r(v_i) = m_i$ we demand

$$\nabla r(v_i) \in \text{span}\{q_1, ..., q_{i+1}\}. \tag{A.14}$$

Again, this can be assured since $r(x)$ decrease most rapidly along its negative gradient. From Eq. (A.12) we see that

$$\nabla r(x) \in \text{span}\{q_1, ..., q_i\}, \tag{A.15}$$

which means that Eq. (A.13) and A.14 are satisfied if

$$\text{span}\{q_1, ..., q_i\} = \text{span}\{q_1, Aq_1, ..., A^{i-1}q_1\}. \tag{A.16}$$

This basis set is often called the Krylov subspace. We could then generate q_{i+1} if it satisfied

$$\text{span}\{q_1, ..., q_{i+1}\} = \text{span}\{q_1, Aq_1, ..., A^{i-1}q_1, A^iq_1\}. \tag{A.17}$$

Finding q_i is now a straightforward job of finding the orthonormal basis of the Krylov subspace. Introducing the Krylov matrix as

$$K(A, q_1, i) = [q_1, Aq_1, ..., A^{i-1}q_1], \tag{A.18}$$

we see that the orthonormal basis of the Krylov subspace is just the column space of the Krylov matrix. If $Q_i^T AQ_i = T_i$ where T is tridiagonal we can write Eq. (A.18) as

$$K(A, q_1, i) = Q[e_1, Te_1, ..., T^{i-1}e_1], \tag{A.19}$$

with

$$Qe_1 = q_1. \tag{A.20}$$

As A is symmetric, so is T. We define the off-diagonal elements of T as $\{b_1, ..., b_{i-1}\}$ and the diagonal elements as $\{a_1, ..., a_i\}$. Doing this we can write out $AQ = QT$ as

$$Aq_j = b_{j-1}q_{j-1} + a_j q_j + b_j q_{j+1}, \tag{A.21}$$

where $j = [1, ..., i-1]$ and $b_0 q_0 = 0$. By using Eq. (A.21), q_{j+1} can be determined. When this is done, Q is known. The method will terminate when $b_j q_{j+1} = 0$. Then, we extract the eigenvalues of T by using an effective symmetric tridiagonal QR algorithm or any other effective diagonalization technique. If for some reason the Q matrix deviates and becomes non-orthogonal we have a problem. This is also the downside of the Lanczos procedure. As we generate the q_i we may run into roundoff errors which could imply that Q becomes non-orthogonal. There are several ways of controlling the orthogonality which we will not cover here. See for example [7]. The computing power of Lanczos methods should not be underestimated as long as our matrix is large and sparse. For an in dept review of effective and practical Lanczos algorithms see [7]. This reference also compares the Lanczos method and the Power method. The Lanczos method is by far superior to the Power method.

A.2 Gauge transformations and invariance

Maxwell's equation are known from classical electromagnetic theory.

$$\nabla \cdot \vec{E} = \rho, \tag{A.22}$$

$$\nabla \times \vec{E} = -\frac{1}{c}\frac{\partial \vec{B}}{\partial t}, \tag{A.23}$$

$$\nabla \cdot \vec{B} = 0, \tag{A.24}$$

$$\nabla \times \vec{B} = \frac{1}{c}\vec{J} + \frac{1}{c}\frac{\partial \vec{B}}{\partial t}, \tag{A.25}$$

where ρ is the charge density, $\vec{J}$ the vector current density. $\vec{B}$ and $\vec{E}$ are the magnetic and electric vector field respectively. Solving Eq. (A.24) and (A.25) with respect to $\vec{B}$ and $\vec{E}$ results in

$$\vec{B} = \nabla \times \vec{A}, \tag{A.26}$$

$$\vec{E} = -\nabla\phi - \frac{1}{c}\frac{\partial \vec{A}}{\partial t}. \tag{A.27}$$

Here, $\vec{A}$ is a vector potential while ϕ is a scalar potential. They are at this time unknown, but should be a function of $\vec{B}$ and $\vec{E}$. Now, consider we do the following transformation

$$\phi \rightarrow \phi' = \phi + \frac{1}{c}\frac{\partial h(\vec{x},t)}{\partial t}, \tag{A.28}$$

$$\vec{A} \rightarrow \vec{A}' = \vec{A} - \nabla h(\vec{x},t), \tag{A.29}$$

where $h(\vec{x},t)$ is a unknown arbitrary function, called gauge function. If we put these transformation back into Eq. (A.26) and (A.29) we see that $\vec{E}$ and $\vec{B}$ is unchanged, whatever $h(\vec{x},t)$ is. Since $\vec{E}$ and $\vec{B}$ is the only observables, we can chose $h(\vec{x},t)$ in any way we want, and still have invariant observables. These type of transformation is known as gauge transformations of second kind. As a consequence of this, all theories using potential ϕ and $\vec{A}$ should be gauge invariant, since the observables does not change. And of this date, there have not been a single valid experiment voiding a gauge invariance. This gives some rules to ϕ and $\vec{A}$. If we input the vector potentials into Eq. (A.22) and (A.23) the following two equations can restrict the choice of $\vec{A}$ and ϕ even more

$$-\nabla^2\phi - \frac{1}{c}\frac{\partial}{\partial t}\left(\nabla\cdot\vec{A}\right) = \rho, \tag{A.30}$$

$$\left(\frac{1}{c^2}\frac{\partial^2}{\partial t^2} - \nabla^2\right)\vec{A} + \nabla\left(\frac{1}{c}\frac{\partial\phi}{\partial t} + \nabla\cdot\vec{A}\right) = \frac{1}{c}\vec{J}. \tag{A.31}$$

Now, we see that due to the freedom of Eq. (A.28) and (A.29) give us the opportunity to chose

$$\nabla\cdot\vec{A} = 0, \tag{A.32}$$

or

$$\nabla\cdot\vec{A} - \frac{1}{c}\frac{\partial\phi}{\partial t}. \tag{A.33}$$

The first one is called Coulomb or transverse gauge, the second Lorentz gauge. The choice of gauge is not restricted to these two, there are many others, but Lorentz and Coulomb gauge are the most frequently used. By a proper gauge function, we can go from a Lorentz gauge to a Coulomb gauge in general. The Coulomb gauge has severe problems in relativistic field calculations since we impose commutator relations between the field to obey the $\vec{x}$ and $\vec{p}$ commutator relation. The manifest Lorentz invariance is also broken if we try to circumvent the problems. Hence the Lorentz gauge is more used due to its covariant form. In this thesis we use the Coulomb gauge, which in this special case is just the same as the Lorentz gauge. We only want a constant magnetic field which means that ρ and $\vec{J}$ can be put to zero. If we impose the Coulomb gauge on Eq. (A.30), we see that the scalar potential $\phi = 0$. From the gauge condition we see that we can chose $\vec{A}$ to be symmetric. We only want a magnetic field along the z-axis and see from Eq. (A.26) that we need a $\vec{A}$ potential with elements in x and y direction, zero otherwise. So if we now chose

$$\vec{A} = \frac{B}{2}\left\{-y, x, 0\right\}. \tag{A.34}$$

We see that $B = B\vec{e}_z$ and Coulomb gauge invariance is not broken.

A.3 Coordinate transformation

Let us now develop the needed transformations from a Cartesian coordinate system to a Polar one. First, we define what is called general curvilinear coordinates. The orthogonal coordinates will be used here. They cover cartesian, polar, spherical and several others. We assume that the functions used in the derivations are continues and differentiable. Let us say that the vector $\vec{r}(x_1, x_2, x_3, ...)$ points at a point in space. Then this vector has tangents as the most elementary basis. We can define them as $\vec{e}_i = \partial\vec{r}/\partial x_i$ for $i = 1, 2, 3, ...$ Each $\vec{e}_i$ will be a tangent to each x_i-curve in a direction of increasing x_i values. If we now normalize these vectors we get

$$\vec{\tilde{e}}_i = \frac{1}{a_i}\frac{\partial\vec{r}}{\partial x_i}. \tag{A.35}$$

Where a_i is the length of each vector. The metric tensor is defined as

$$g_{ij} = \frac{\partial\vec{r}}{\partial x_i}\frac{\partial\vec{r}}{\partial x_j}. \tag{A.36}$$

In the orthogonal case g_{ij} is a matrix with a_i^2 on the diagonal. An infinitesimal displacement along $\vec{r}$ in three dimensions can be written as

$$d\vec{r} = \frac{\partial\vec{r}}{\partial x_1}dx_1 + \frac{\partial\vec{r}}{\partial x_2}dx_2 + \frac{\partial\vec{r}}{\partial x_3}dx_3, \tag{A.37}$$

in terms of $\vec{\tilde{e}}_i$ we get

$$d\vec{r} = a_1 dx_1\vec{\tilde{e}}_1 + a_2 dx_2\vec{\tilde{e}}_2 + a_2 dx_2\vec{\tilde{e}}_2. \tag{A.38}$$

We introduce a vector potential $\psi(x_1, x_2, x_3, ...)$. A infinitesimal change in three dimensions in x_i gives the change of ψ as follows

$$d\psi = \frac{\partial\psi}{\partial x_2}dx_1 + \frac{\partial\psi}{\partial x_2}dx_2 + \frac{\partial\psi}{\partial x_3}dx_3. \tag{A.39}$$

Comparing this result with Eq. (A.37), we observe that we can write

$$d\psi = \nabla\psi \cdot d\vec{r}, \tag{A.40}$$

where

$$\nabla\psi = \frac{\vec{\tilde{e}}_1}{a_1}\frac{\partial\psi}{\partial x_1} + \frac{\vec{\tilde{e}}_2}{a_2}\frac{\partial\psi}{\partial x_2} + \frac{\vec{\tilde{e}}_3}{a_3}\frac{\partial\psi}{\partial x_3}, \tag{A.41}$$

giving the *nabla* operator

$$\nabla = \frac{\vec{\tilde{e}}_1}{a_1}\frac{\partial}{\partial x_1} + \frac{\vec{\tilde{e}}_2}{a_2}\frac{\partial}{\partial x_2} + \frac{\vec{\tilde{e}}_3}{a_3}\frac{\partial}{\partial x_3}. \tag{A.42}$$

We have now developed an general expression for the gradient and del operator in three dimension curvilinear coordinates. We also need the divergence to

calculate the Laplace operator. Define a vector field

$$\vec{f} = f_1\vec{e}_1 + f_2\vec{e}_2 + f_3\vec{e}_3, \tag{A.43}$$

calculate the divergence

$$\nabla \cdot \vec{f} = \nabla \cdot (f_1\vec{e}_1) + \nabla \cdot (f_2\vec{e}_2) + \nabla \cdot (f_3\vec{e}_3). \tag{A.44}$$

Observing what will happen to the first term if we write it out

$$\nabla \cdot (f_1\vec{e}_1) = \frac{\partial f_1}{\partial x_1} + f_1\left(\frac{\partial \vec{e}_1}{\partial x_1}\right)\vec{e}_1. \tag{A.45}$$

The last term is problematic since we have no direct way of calculating it. Calculate the gradient of x_1 by using the developed term for the del operator in Eq. (A.42)

$$\nabla x_1 = \frac{1}{a_1}\vec{e}_1, \tag{A.46}$$

and similar for the other two components. We also note that

$$\vec{e}_1 = \vec{e}_2 \times \vec{e}_3, \tag{A.47}$$

which gives, using Eq. (A.46)

$$\vec{e}_1 = a_2\nabla x_2 \times a_3\nabla x_3. \tag{A.48}$$

Again we write out the first term in Eq. (A.44), but now with the help of Eq. (A.48)

$$\nabla \cdot (f_1\vec{e}_1) = \nabla(f_1a_2a_3) \cdot (\nabla x_2 \times \nabla x_3) + f_1a_2a_3\nabla \cdot (\nabla x_2 \times \nabla x_3), \tag{A.49}$$

writing out the last term, we see that

$$\nabla \cdot (\nabla x_2 \times \nabla x_3) = \nabla x_3 \cdot (\nabla \times \nabla x_2) - \nabla x_2 \cdot (\nabla \times \nabla x_3), \tag{A.50}$$

is $\vec{0}$ since $\nabla \times \nabla x_i = \vec{0}$. Using Eq. (A.46) again we get

$$\nabla \cdot (f_1\vec{e}_1) = \frac{1}{a_2a_3}(\vec{e}_2 \times \vec{e}_3)\nabla(f_1a_2a_3), \tag{A.51}$$

using Eq. (A.47) and Eq. (A.42) gives

$$\nabla \cdot (f_1\vec{e}_1) = \frac{\vec{e}_1}{a_2a_3}\left(\frac{\vec{e}_1}{a_1}\frac{\partial}{\partial x_1}(f_1a_2a_3)\right). \tag{A.52}$$

This is of course cyclic in the coordinates and we can finally write out the divergence in Eq. (A.44) as

$$\nabla \cdot \vec{f} = \frac{1}{a_1a_2a_3}\left(\frac{\partial}{\partial x_1}(f_1a_2a_3) + \frac{\partial}{\partial x_2}(f_2a_1a_3) + \frac{\partial}{\partial x_3}(f_3a_1a_2)\right) \tag{A.53}$$

We need a general expression for the Laplace operator. This is rather simple. We can set $\vec{f} = \nabla$ in the equation above and get

$$\nabla^2 = \frac{1}{a_1 a_2 a_3}\left(\frac{\partial}{\partial x_1}\left(\frac{a_2 a_3}{a_1}\frac{\partial}{\partial x_1}\right) + \frac{\partial}{\partial x_2}\left(\frac{a_1 a_3}{a_2}\frac{\partial}{\partial x_2}\right) + \frac{\partial}{\partial x_3}\left(\frac{a_1 a_2}{a_3}\frac{\partial}{\partial x_3}\right)\right) \tag{A.54}$$

The volume element in three dimensions are given as

$$dV = a_1 a_2 a_3 dx_1 dx_2 dx_3. \tag{A.55}$$

Expressions for cylindrical polar coordinates can now be developed. First define

$$x = rcos(\theta), \tag{A.56}$$
$$y = rsin(\theta), \tag{A.57}$$
$$z = z, \tag{A.58}$$

where r is the radial distance from the origin to the point P, while θ is the anticlockwise angle from the x-axis up to P. The last coordinate z is the same as in the Cartesian case. Transforming the vector $\vec{r}$ from Cartesian to polar coordinates results in the following $\vec{r}$

$$\vec{r} = \begin{bmatrix} rcos(\theta) \\ rsin(\theta) \\ z \end{bmatrix}. \tag{A.59}$$

We need to calculate the normalizations variables. Remember that

$$a_i = \left\| \frac{\partial \vec{r}}{\partial x_i} \right\|. \tag{A.60}$$

This gives

$$a_r = 1, \tag{A.61}$$
$$a_\theta = r, \tag{A.62}$$
$$a_z = 1. \tag{A.63}$$

We put this into Eq. (A.54) and get

$$\nabla^2 = \frac{1}{r}\left(\frac{\partial}{\partial r}\left(r\frac{\partial}{\partial r}\right)\right) + \frac{1}{r^2}\frac{\partial^2}{\partial \theta^2} + \frac{\partial^2}{\partial z^2}. \tag{A.64}$$

Observe that in we could also write out the first term as a second and first derivate. In the two-dimensional case this would be

$$\nabla^2 = \frac{\partial^2}{\partial r^2} + \frac{1}{r}\frac{\partial}{\partial r} + \frac{1}{r^2}\frac{\partial^2}{\partial \theta^2}. \tag{A.65}$$

The volume element in two dimensional cylindrical polar coordinates are

$$dV = rdrd\theta. \tag{A.66}$$

In spherical polar coordinates we define

$$x = rcos(\theta)sin(\phi), \tag{A.67}$$
$$y = rsin(\theta)sin(\phi), \tag{A.68}$$
$$z = rcos(\phi). \tag{A.69}$$

When we now transform the vector $\vec{r}$ from Cartesian to spherical polar coordinates we get

$$\vec{r} = \begin{bmatrix} rcos(\theta)sin(\phi) \\ rsin(\theta)sin(\phi) \\ rcos(\phi) \end{bmatrix}. \tag{A.70}$$

From Eq. (A.60) we see that

$$a_r = 1, \tag{A.71}$$
$$a_\theta = rsin(\phi), \tag{A.72}$$
$$a_\phi = r. \tag{A.73}$$

Plugging this into Eq. (A.54) give us the Laplace operator for the spherical polar case as follows

$$\nabla^2 = \frac{1}{r^2}\frac{\partial}{\partial r}\left(r^2\frac{\partial}{\partial r}\right) + \frac{1}{r^2 sin^2(\theta)}\frac{\partial^2}{\partial\theta^2} + \frac{1}{r^2 sin(\phi)}\frac{\partial}{\partial\phi}\left(sin(\phi)\frac{\partial}{\partial\phi}\right), \tag{A.74}$$

which also can be written

$$\nabla^2 = \frac{\partial^2}{\partial r^2} + \frac{2}{r}\frac{\partial}{\partial r} + \frac{1}{r^2 sin^2(\theta)}\frac{\partial^2}{\partial\theta^2} + \frac{cot(\phi)}{r^2}\frac{\partial}{\partial\phi} + \frac{1}{r^2}\frac{\partial^2}{\partial\phi^2}. \tag{A.75}$$

The volume element in spherical polar coordinates are

$$dV = r^2 sin(\phi) dr d\theta d\phi. \tag{A.76}$$

In this thesis we have introduced the angular momentum. We will now develop an expression for the z-component and the squared of the angular momentum. We know that

$$\vec{L} = \vec{r} \times \vec{p}, \tag{A.77}$$

written in components

$$L_x = yp_z - zp_y, \tag{A.78}$$
$$L_y = zp_x - xp_z, \tag{A.79}$$
$$L_z = xp_y - yp_x. \tag{A.80}$$

We now transform this into polar coordinates as we did with the Laplace operator. Let us first do this in three dimensions, since the two dimensional case is easily derived from this. By the substitution $p_x \rightarrow -i\hbar\partial/\partial x$ and the analogy, we can write the angular momentum components as

$$L_z = -i\hbar\left(x\frac{\partial}{\partial y} - y\frac{\partial}{\partial x}\right). \tag{A.81}$$

Just like Eq. (A.39) we can write

$$\frac{\partial\psi}{\partial x} = \frac{\partial r}{\partial x}\frac{\partial\psi}{\partial r} + \frac{\partial\theta}{\partial x}\frac{\partial\psi}{\partial\theta} + \frac{\partial\phi}{\partial x}\frac{\partial\psi}{\partial\phi}. \tag{A.82}$$

With the analogy for the y and z derivatives. Using the same $\vec{r}$ as in Eq. (A.70) with any given vector potential ψ gives

$$\frac{\partial\psi}{\partial x} = cos(\theta)sin(\phi)\frac{\partial\psi}{\partial r} + \frac{cos(\theta)cos(\phi)}{r}\frac{\partial\psi}{\partial\theta} - \frac{sin(\theta)}{rsin(\phi)}\frac{\partial\psi}{\partial\phi}, \tag{A.83}$$

$$\frac{\partial\psi}{\partial y} = sin(\theta)sin(\phi)\frac{\partial\psi}{\partial r} + \frac{sin(\theta)cos(\phi)}{r}\frac{\partial\psi}{\partial\theta} - \frac{cos(\theta)}{rsin(\phi)}\frac{\partial\psi}{\partial\phi}. \tag{A.84}$$

Now substitute the derivatives back into Eq. (A.81) we immediately see that the angular momentum operator in polar coordinates are

$$L_z = -i\hbar\frac{\partial}{\partial\theta} \tag{A.85}$$

The remaining part of this section is to show an expression for the angular momentum squared. The angular momentum is a vector and therefore we can write

$$L^2 = L_x^2 + L_y^2 + L_z^2. \tag{A.86}$$

Calculating this involves a lot of algebra. First we need to substitute the derivative transformations back into all three angular momentum components, then take the squared and sum them together. The final result is

$$L^2 = -\hbar^2\left(\frac{1}{sin^2(\phi)}\frac{\partial^2}{\partial\theta^2} + cot(\phi)\frac{\partial}{\partial\phi} + \frac{\partial^2}{\partial\phi^2}\right) \tag{A.87}$$

A.4 Time-independent perturbation theory

Time-independent perturbation theory has a wide range of application and its basics will be covered in this section. The whole idea of perturbation theory is to threat a problem as two parts. The first part is known and can be calculated, while the second is unknown and small compared to the first. Using Hamiltonian operators we can write

$$H = H_0 + \lambda H_1. \tag{A.88}$$

Where H_0 has a known solution, H_1 has not. The constant λ will give the order of perturbation later. Often H_1 are referred to as the correction term or as a perturbation. We define, in Dirac notation

$$H_0|n_0\rangle = E_0|n_0\rangle. \tag{A.89}$$

Where $|n_0\rangle$ are the normalized eigenvector and E_0 are the eigenvalue of H_0. In this thesis we will only meet non-degenerate eigenvalues. Degenerate perturbation theory is not covered in this thesis. Assume that we can expand the eigenvectors and eigenvalues in the parameter λ

$$|n\rangle = |n^0\rangle + \lambda|n^1\rangle + \lambda^2|n^2\rangle + ..., \tag{A.90}$$

$$E_n = E_n^0 + \lambda E_n^1 + \lambda^2 E_n^2 + ... \tag{A.91}$$

The exact eigensolutions are given as

$$H|n\rangle = E_n|n\rangle. \tag{A.92}$$

Substituting Eq. (A.89) into the equation over gives

$$(H_0 + \lambda H_1)|n\rangle = E_n|n\rangle. \tag{A.93}$$

Expanding and moving eigenvalues from right to left gives

$$(H_0 + \lambda H_1 - E_n^0 - \lambda E_n^1 - \lambda^2 E_n^2 + ...)(|n^0\rangle + \lambda|n^1\rangle + \lambda^2|n^2\rangle + ...) = 0. \tag{A.94}$$

This equation should be valid for all λ thus giving rise to equations of different orders. The first few are given in Tab. A.4.13 The first equation are already

Order, λ	Equation
0	$(H_0 - E_0)\|n^0\rangle = 0$
1	$(H_0 - E_0)\|n^1\rangle + (H_1 - E_n^1)\|n^0\rangle = 0$
2	$(H_0 - E_n^0)\|n^2\rangle + (H_1 - E_n^1)\|n^1\rangle + E_n^2\|n^0\rangle = 0$

Table A.4.13: Lowest order perturbation equations.

assumed. If we multiply the equation corresponding to $\lambda = 1$ with $\langle n^0|$ from the left and make use of $\langle n_0|n_0\rangle = 1$ we get

$$\langle n^0|H_0 - E_n^0|n^1\rangle + \langle n^0|H_1|n^0\rangle - E_n^1 = 0, \tag{A.95}$$

where we can write

$$\langle n^0|H_0 - E_n^0|n^1\rangle = \langle n^1|H_0 - E_n^0|n^0\rangle^\dagger, \tag{A.96}$$

which is zero from Tab. A.4.13. We now have an expression for the first order eigenvalue correction given as

$$E_n^1 = \langle n^0|H_1|n^0\rangle. \tag{A.97}$$

To find the first order eigenvector correction we multiply the first order equation with $\langle n'|$, $n' \neq n$ from the left and make use of $\langle i|j\rangle = \delta_{ij}$. We then get

$$\langle n'|H_0 - E_n^0|n^1\rangle + \langle n'|H_1|n^0\rangle. \tag{A.98}$$

Let us complex conjugate the first term

$$\langle n'|H_0 - E_n^0|n^1\rangle = \langle n^1|H_0 - E_n^0|n'\rangle^\dagger, \tag{A.99}$$

and use $H_0|n'\rangle = E_{n'}^0|n'\rangle$ to get

$$\langle n'|H_0 - E_n^0|n^1\rangle = (E_{n'}^0 - E_n^0)\langle n'|n^1\rangle. \tag{A.100}$$

Solving this equation and using the completeness relation to expand the eigenvector gives

$$|n^1\rangle = \sum_{n' \neq n} \frac{\langle n'|H_1|n^0\rangle}{E_n^0 - E_{n'}^0}|n'\rangle. \tag{A.101}$$

In many situations the second order term are needed. We can obtain the expression for E_n^2 by multiplying the second order equation in Tab. A.4.13 with $\langle n^0|$ from the left. This give rise to

$$\langle n^0|H_0 - E_n^0|n^2\rangle + \langle n^0|H_1 - E_n^1|n^1\rangle - E_n^2 = 0, \tag{A.102}$$

where the first term is zero by using complex conjugation. Solving for E_n^2 yields

$$E_n^2 = \langle n^0|H_1|n^1\rangle. \tag{A.103}$$

By substituting Eq. (A.101) into the equation above we get

$$E_n^2 = \sum_{n' \neq n} \frac{\langle n'|H_1|n^0\rangle\langle n^0|H_1|n'\rangle}{E_n^0 - E_{n'}^0}. \tag{A.104}$$

By complex conjugation we can write the second order eigenvalues perturbation as

$$E_n^2 = \sum_{n' \neq n} \frac{|\langle n'|H_1|n^0\rangle|^2}{E_n^0 - E_{n'}^0}. \tag{A.105}$$

We will not be using the eigenvector perturbations explicitely nor any higher order eigenvalue perturbations. Thus we will not develop an expression for the second order eigenvector perturbation. Writing out the eigenvalue to second order from Eq. (A.91) gives

$$E_n = E_n^0 + \langle n^0|H_1|n^0\rangle + \sum_{n' \neq n} \frac{|\langle n'|H_1|n^0\rangle|^2}{E_n^0 - E_{n'}^0} + O(\lambda^3). \tag{A.106}$$

The perturbation theory we just considered are called Rayleigh-Schrödinger perturbation theory. It has one advantage and one disadvantage over Brillouin-Wigner perturbation theory (FINN REF). The disadvantage is that we may have get divergence if we have degenerate energy levels. However, Brillouin-Wigner perturbation theory gives implicit equation since the denominator includes E_n. For the perturbation theory to be valid, the series in Eq. (A.101) need to converge. We then require

$$\left|\frac{\langle n'|H_1|n^0\rangle}{E_n^0 - E_{n'}^0}\right| \ll 1. \tag{A.107}$$

A.5 Numerical Integration

In this section we will discuss different numerical integrations techniques and at the end decide which of those are best suited to our application. Basically we want to calculate

$$I = \int_i^e f(x)dx. \tag{A.108}$$

The integral starts at $x = i$ and ends at $x = e$. It is well known that integrals compute the areal under a graph with boundary conditions set up by i, e and the coordinate axis.

A.5.1 Equal width techniques

As the most simple approximation we could divide the area into a given number of bars as shown in Fig. A.5.19. By making the bar width, which we define as

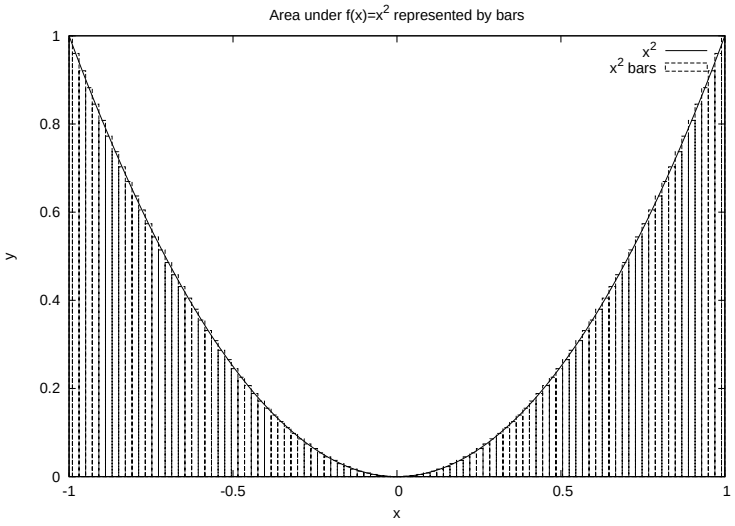

Figure A.5.19: Area of $f(x) = x^2$ represented by bars

h smaller and smaller, the approximation becomes better. This approximation is very simple and accuracy suffer unless h is very small, especially if $f(x)$ have large derivatives. It is crucial that $f(x)$ is a smooth function over the interval and have well defined derivatives. Let us now partition Eq. (A.108) as

$$\int_i^e f(x)dx = \int_i^{i+h} f(x)dx + \int_{i+h}^{i+2h} f(x)dx + ... + \int_{e-h}^{e} f(x)dx. \qquad \text{(A.109)}$$

. Let us look closer at the integral over the first interval. By approximating $f(x)$ as a linear function between i and $i + h$ we get trapezoids instead of bars. Hence this integration technique are often referred to as the "Trapezoidal rule". The average height between the two endpoints in the sub-interval is $(f(i) + f(i + h))/2$. To get the area, we need to multiply the height by the width, which is h. Doing this we get

$$\int_i^{i+h} f(x)dx \approx \frac{h}{2}(f_i + f_{i+1}). \qquad \text{(A.110)}$$

Where f_i and f_{i+1} are evaluated at point $x = i$ and $x = i + h$ respectively. On the interval [i,e] the integral approximation becomes

$$\int_i^e f(x)dx = h\left(\frac{f(i)}{2} + f(i+h) + f(i+2h) + ... + f(e-h) + \frac{f(e)}{2}\right). \tag{A.111}$$

Only the endpoints keep their pre-factor of $1/2$ since the internal points are counted twice. From a more general viewpoint we could write Eq. (A.108) as

$$\int_i^e f(x)dx = \sum_{i=1}^{N} f_i w_i. \tag{A.112}$$

Comparing this to Eq. (A.110) we have $N = 2$ and $w_1 = w_2 = h/2$. Other approximation than the Trapezoidal rule can be found if we represent $f(x)$ by a higher degree polynomial between the points. In Tab. A.5.14 we have listed the most common numerical integration techniques using equal width.

	N	w_i
Trapezoid	1	$(h/2, h/2)$
Simpson's	2	$(h/3, 4h/3, h/3)$
Simpson's 3/8	3	$(3h/8, 9h/8, 9h/8, 3h/8)$
Bodes	4	$(14h/45, 64h/45, 24h/45, 64h/45, 14h/45)$

Table A.5.14: Equal width numerical integration techniques.

Later we are going to investigate the numerical error in these methods, but first we need to determine the analytical error. To find this we use a Taylor expansion [18] around a point $x = a$ given as

$$f_{a+b} = f_a + b\frac{df_a}{dx} + \frac{b^2}{2}\frac{d^2f_a}{dx^2} + \frac{b^3}{8}\frac{d^3f_a}{dx^3} + O(h^4). \tag{A.113}$$

Let $a = i+1/2$ and $b = \pm 1/2$ to get the Taylor expansion around the half-width of h for one sub-interval as

$$f_{i+1/2,\pm 1/2} = f_{i+1/2} \pm \frac{1}{2}\frac{df_{i+1/2}}{dx} + \frac{1}{8}\frac{d^2f_{i+1/2}}{dx^2} \pm \frac{1}{48}\frac{d^3f_{i+1/2}}{dx^3} + O(h^4). \tag{A.114}$$

Combining this with Eq. (A.110) we get

$$\int_i^{i+1} f(x)dx \approx h\left(f_{i+1/2} + \frac{h^2}{8}\frac{d^2f_{i+1/2}}{dx^2} + O(h^4)\right). \tag{A.115}$$

To be able to separate the error we need an exact expression for the integration within one sub-interval. For comparison reasons we choose to evaluate this integral around $x = i + h/2$. This gives, after a variable change

$$\int_i^{i+1} f(x)dx = \int_{-h/2}^{h/2} f(x_{i+1/2} + t)dt. \tag{A.116}$$

Taylor expansion is again used on $f(x_{i+1/2}+t)$ to give

$$\int_{-h/2}^{h/2} f(x_{i+1/2}+t)dt = \int_{-h/2}^{h/2} \sum_{n=0}^{\infty} f_{i+1/2}^{(n)} \frac{t^n}{n!} dt. \tag{A.117}$$

Where $f^{(n)}$ is the n'the derivative of f. The change in notation should be obvious from earlier derivations. Evaluating the integral give us an exact expression for the integrals as follows

$$\int_{-h/2}^{h/2} f(x_{i+1/2}+t)dx = \sum_{\substack{n=0 \\ even}}^{\infty} f_{i+1/2}^{(n)} \frac{2}{(n+1)!} \left(\frac{h}{2}\right)^{n+1}. \tag{A.118}$$

Subtract Eq. (A.115) from this, we get the analytical local error

$$E_l = \frac{h^3}{12} \frac{d^2 f_{i+1/2}}{dx^2} + O(h^5). \tag{A.119}$$

If we take N as the number of sub-intervals we can write

$$h = \frac{e-i}{N}. \tag{A.120}$$

The local error will be added N times. The global error will be the total analytical error on the interval [i,e]. This can now be approximated as

$$E_g \approx \frac{(e-i)^3}{12N^2} \frac{d^2 f_{i+1/2}}{dx^2}. \tag{A.121}$$

Similar expression can be found for the other integration techniques by using the same procedures. The Trapezoidal rule give exact solutions for linear $f(x)$ on the sub-interval just as the Simpson's rule give us exact solutions for parabolic $f(x)$. On the global scale we can at best hope for an exact solution of a $N-1$ degree polynomial by using N points. In this thesis we are going to integrate polynomials with much higher orders than one and two. It is possible to improve the accuracy by using Gaussian quadrature integration.

A.5.2 Gaussian quadrature techniques

We will see that often Gaussian quadrature offer a faster and more accurate integration scheme than the equal width techniques. But in some cases the Simpson's rule can yield better results. This if often the case if our function have noise embedded to it. The choice of method depends on the behavior of $f(x)$. As before we can write the integral as

$$\int_i^e f(x)dx = \sum_{i=1}^{N} f_i w_i. \tag{A.122}$$

Let us now be more open minded than previous. By not fixing the integration points and weights we have greater flexibility to choose the variables. Actually the approximation error vanish if we choose correct weights and $f(x)$ is a $2N-1$ degree polynomial. This is due to the fact that we have N different

mesh points and weights give rise to $2N$ degrees of freedom. It is important that $f(x)$ is smooth, or can be made smooth by factoring out $g(x)$ from $f(x)$ as $f(x) = g(x)F(x)$. Singularities or unwanted behavior is included in $g(x)$, thus making $F(x)$ more smooth. In Tab. A.5.15 we have listed the most used Gaussian quadrature integration techniques. We will not go into the procedures

	Integral	$g(x)$
Gauss-Legendre	$\int_a^b f(x)dx$	1
Gauss-Chebyshev	$\int_{-1}^{1} \frac{1}{\sqrt{1-x^2}} F(x)dx$	$\frac{1}{\sqrt{1-x^2}}$
Gauss-Hermite	$\int_{-\infty}^{\infty} e^{-x^2} F(x)dx$	e^{-x^2}
Gauss-Laguerre	$\int_0^{\infty} x^\alpha e^{-x^2} F(x)dx$	$x^\alpha e^{-x^2}$
Gauss-Jacobi	$\int_{-1}^{1} (1-x)^\alpha (1+x)^\beta F(x)dx$	$(1-x)^\alpha (1+x)^\beta$

Table A.5.15: Overview of Gaussian quadrature integration techniques. α and β are constants.

of calculating the integration points and weights. For details see [14]. Immediately we recognize the Laguerre behavior we obtained by solving the harmonic oscillator problem. The Gauss-Laguerre integration technique will therefore be used in further discussions.

A.5.3 Numerical analysis of the numerical integration techniques

The discussion in the last section yielded different integrations techniques. In this section we will create a test case and compare the trapezoidal, Simpson's and Gauss-Laguerre techniques. At the end we will hopefully come to a conclusion of the preferred method. In this thesis $F(x)$ would be the Laguerre polynomials. To be able to compere results, we also need the analytical solution. For simplicity we chose to integrate

$$\int_0^{\infty} x^\alpha e^{-x^2} (1 - x^2 + x^4) dx. \tag{A.123}$$

As this reflect our Laguerre solutions. We will the expression in brackets a $p = 4$ polynomial for further reference. From definite integral tables (FINN REF) we know that

$$\int_0^{\infty} x^\alpha e^{-\beta x^2} dx = \frac{1}{2} \beta^{-(\alpha+1)/2} \Gamma\left(\frac{\alpha+1}{2}\right). \tag{A.124}$$

Using this, Eq. (A.123) have the analytical solution

$$\int_0^{\infty} x^\alpha e^{-x^2} (1 - x^2 + x^4) dx = \frac{1}{2}\left[\Gamma\left(\frac{\alpha+1}{2}\right) - \Gamma\left(\frac{\alpha+3}{2}\right) + \Gamma\left(\frac{\alpha+5}{2}\right)\right]. \tag{A.125}$$

In Fig. A.5.20 we have compared the relative error using three integration techniques. Each figure represent a given order of integration polynomial p. We clearly see that the Gauss-Laguerre method is stable, even for very low n. As p increase the equal width methods need more integration points to keep up with the Gauss-Laguerre technique. This should not come as a surprise, since the complexity increase with p. Gauss-Laguerre methods are also more computer

efficient to calculate. Remember that in the case of Gauss-Laguerre integration techniques we substitute $y = x^2$. Taking this into account, we should be able to integrate an order p polynomial using $n = (p+2)/4$ integration points exactly. By exact, we mean up to numerical precision. This behavior can be observed in Fig. A.5.20. In this thesis we have strictly used Gauss-Laguerre due to its

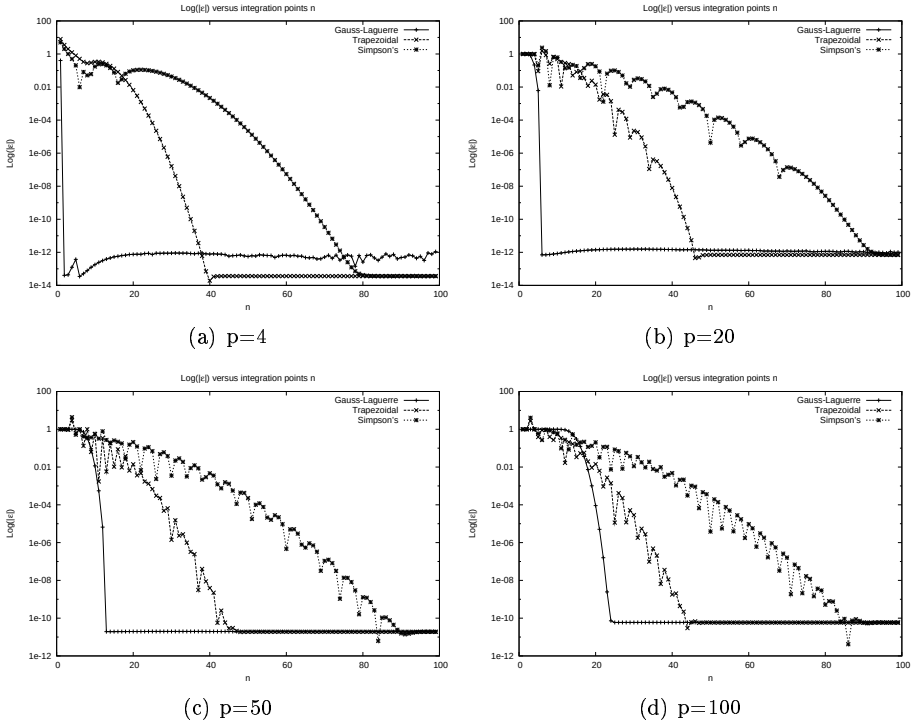

(a) p=4 (b) p=20

(c) p=50 (d) p=100

Figure A.5.20: The logarithm of the error $|\epsilon|$ as a function of numerical integration points n.

simplicity and effectiveness.

A.6 Solution of the radial equation

In the first part of this section we will look at the two dimensional case. The three dimensional solutions are worked out at the end.

A.6.1 Two dimension

We will now solve the Schrödinger equation given as

$$-\frac{\hbar^2}{2m^*}\left(\frac{\partial^2}{\partial r^2}+\frac{1}{r}\frac{\partial}{\partial r}-\frac{m^2}{r^2}-\frac{emB}{\hbar c}\right)\psi(r)+\frac{1}{2}m^*\omega^2 r^2\psi(r)=E\psi(r). \quad \text{(A.126)}$$

Define

$$\epsilon=\frac{2m^*E}{\hbar^2}-\frac{emB}{\hbar c}, \quad \text{(A.127)}$$

and substitute

$$x = r^2, \tag{A.128}$$

into Eq. (A.126) to get

$$-\left(4x\frac{\partial^2}{\partial x^2}+4\frac{\partial}{\partial x}-\frac{m^2}{x}\right)\psi'(x)+\frac{m^{*2}\omega^2}{\hbar^2}x\psi'(x)=\epsilon\psi'(x). \tag{A.129}$$

To get rid of the first derivative we can do the substitution $\psi'(x)=x^{-1/2}u(x)$. After a bit of algebra we get the equation

$$-\frac{\partial^2 u(x)}{\partial x^2}+\frac{1}{4}\left(\frac{m^{*2}\omega^2}{\hbar^2}-\frac{\epsilon}{x}-\frac{(1-m^2)}{x^2}\right)u(x)=0. \tag{A.130}$$

To make the equation dimensionless, substitute $y=m^*\omega x/\hbar=\beta x$. This gives

$$-\frac{\partial^2 u'(y)}{\partial y^2}+\frac{1}{4}\left(1-\frac{\epsilon}{\beta y}-\frac{(1-m^2)}{y^2}\right)u'(y)=0. \tag{A.131}$$

We now have a much simpler equation compared to what we started out with. However, we still need to make some general considerations in the limits to get to the wanted solutions. Let us consider what is going on if we let $y\to\infty$. When this happens we get a very simple equation

$$\frac{\partial^2 u'(y)}{\partial y^2}\simeq\frac{1}{4}u'(y), \tag{A.132}$$

which have a approximate solution which goes as $u'(y)\simeq e^{\pm y/2}$. But we need the solution to be finite, even at $y\to\infty$. Then, only the solution for the negative y is allowed. That is

$$u'(y)\simeq e^{-y/2}. \tag{A.133}$$

Now, let us consider $y\to 0$. In this regime we get a equation

$$\frac{\partial^2 u'(y)}{\partial y^2}\simeq\frac{m^2-1}{4y^2}u'(y). \tag{A.134}$$

This equation has two solution

$$u'(y) \simeq y^{(m+1)/2}, \tag{A.135}$$
$$u'(y) \simeq y^{-(m-1)/2}. \tag{A.136}$$

Since this should be finite at $y=0$ and if $m>0$ we see that the only valid solution is the first. Combining Eq. (A.133) and Eq. (A.135) we can now substitute

$$u'(y)=y^{(m+1)/2}e^{-y/2}\rho(y), \tag{A.137}$$

into Eq. (A.131) and get, again after tedious algebra

$$y\frac{\partial^2 p(y)}{\partial y^2}+(m+1-y)\frac{\partial p(y)}{\partial y}+\frac{1}{2}\left(\frac{\epsilon}{2\beta}-m-1\right)p(y)=0. \tag{A.138}$$

Define

$$\lambda = \frac{1}{2}\left(\frac{\epsilon}{2\beta} - m - 1\right), \tag{A.139}$$

and substitute into the previous differential equation

$$y\frac{\partial^2 p(y)}{\partial y^2} + (m+1-y)\frac{\partial p(y)}{\partial y} + \lambda p(y) = 0. \tag{A.140}$$

We have now arrived at a differential equation known as the associated Laguerre differential equation. Its solutions can be found by series expansion. Let us do this for illustrative purpose. The quantum number n will arise during termination of the series and hence it is important. From Eq. (A.140) we see that there is a singular point at $y = 0$ and a irregular singularity at $y = \infty$. From Fuch's theorem (FINN REF), we know that there exist a solution by using the Frobenius series

$$p(y) = \sum_{n=0}^{\infty} a_n y^{n+\sigma} \tag{A.141}$$

Where σ is any number and a_n are constants to be determined. Now, derivate $p(y)$ twice to get

$$\frac{\partial p(y)}{\partial y} = \sum_{n=0}^{\infty}(n+\sigma)a_n y^{n+\sigma-1}, \tag{A.142}$$

$$\frac{\partial^2 p(y)}{\partial y^2} = \sum_{n=0}^{\infty}(n+\sigma)(n+\sigma-1)a_n y^{n+\sigma-2}. \tag{A.143}$$

We now demand that $a_0 \neq 0$ since if this was not the case, we could redefine σ to make $a_0 \neq 0$. Putting equation Eq. (A.141), (A.142) and Eq. (A.143) into Eq. (A.140) we get

$$\begin{aligned} y\sum_{n=0}^{\infty}(n+\sigma)(n+\sigma-1)a_n y^{n+\sigma-2} + (m+1)\sum_{n=0}^{\infty}(n+\sigma)a_n y^{n+\sigma-1} \quad - \\ -y\sum_{n=0}^{\infty}(n+\sigma)a_n y^{n+\sigma-1} + \lambda\sum_{n=0}^{\infty}a_n y^{n+\sigma} = 0, \end{aligned} \tag{A.144}$$

divide by $y^{\sigma-1}$ to get

$$\begin{aligned} \sum_{n=0}^{\infty}(n+\sigma)(n+\sigma-1)a_n y^{n} + (m+1)\sum_{n=0}^{\infty}(n+\sigma)a_n y^{n} \quad - \\ -\sum_{n=0}^{\infty}(n+\sigma)a_n y^{n+1} + \lambda\sum_{n=0}^{\infty}a_n y^{n+1} = 0, \end{aligned} \tag{A.145}$$

sort terms so that

$$\sum_{n=0}^{\infty}\left[(n+\sigma)(n+\sigma-1) + (m+1)(n+\sigma) + y(\lambda - n - \sigma)\right]a_n y^n = 0. \tag{A.146}$$

This equation should be valid for all y. Setting $y = 0$ we see that all therms with $n > 0$ vanish. Remember that we demanded that $a_0 \neq 0$. We can then remove the remaining a_0 giving rise to the indicial equation

$$\sigma(\sigma + m) = 0 \tag{A.147}$$

We see that the solutions are $\sigma = 0$ or $\sigma = -m$. As things are in physics we don't want divergent solutions. m is a integer. We can not accept a solution with $\sigma = -m$ around $y = 0$. We then consider the remaining option. Putting $\sigma = 0$ back into equation Eq. (A.145) gives

$$\sum_{n=0}^{\infty} n(n-1)a_n y^n + (m+1)\sum_{n=0}^{\infty} n a_n y^n - \sum_{n=0}^{\infty} n a_n y^{n+1} + \lambda \sum_{n=0}^{\infty} a_n y^{n+1} = 0, \tag{A.148}$$

doing variable change and sorting terms to get

$$\sum_{n=0}^{\infty} \left\{ [(n+1)n + (m+1)(n+1)]\, a_{n+1} + [\lambda - n]\, a_n \right\} y^n = 0. \tag{A.149}$$

This equation is satisfied if the coefficient of each power of y vanish separately. This gives the recurrence relation

$$a_{n+1} = \frac{n - \lambda}{(n+1)(m+n+1)} a_n. \tag{A.150}$$

This equation determines the coefficients of the general solution in Eq. (A.141). Expanding, by substituting Eq. (A.150) into Eq. (A.141) we get

$$p(y) = \left[1 - \frac{\lambda}{m+1} y - \frac{(1-\lambda)\lambda}{2(m+2)(m+1)} y^2 + ... \right] a_0 \tag{A.151}$$

As long as $\lambda \geq 0$ the series converges. Also, we want the series to terminate at a given n because of normalizability. This happens when $n - \lambda = 0$. Since n is integer, λ is to. Relabeling $\lambda = n$ we get the allowed values for n

$$n = 0, 1, 2, 3, ... \tag{A.152}$$

We still need to determine a_0. Looking at Eq. (A.140) we see that $p(y)$ can be multiplied with any constant and still be a solution. Since there exist a solution for each m and n, we can choose this constant to be different for each solution. From Eq. (A.151) we also see that $m \geq 0$ to have a non-divergent solution. This gives the associated Laguerre polynomials $L_n^{|m|}$ as solution to Eq. (A.140). The first few are listed in Tab. A.6.16. The Rodrigues (FINN REF, mathworld)

n	$L_n^{\lvert m\rvert}(y)$
0	1
1	$-y + \lvert m\rvert + 1$
2	$\frac{1}{2}\left(\lvert m\rvert + 1)(\lvert m+2\rvert) - 2(\lvert m\rvert + 2)y + y^2\right)$

Table A.6.16: Lowest order associated Laguerre polynomials.

representation of the associated Laguerre polynomials are

$$L_n^{|m|}(y) = \frac{e^y y^{-|m|}}{n!}\frac{\partial^n}{\partial y^n}\left(e^{-y}y^{n+|m|}\right). \tag{A.153}$$

We may also write the Laguerre polynomials as a finite series (FINN REF, mathworld)

$$L_n^{|m|}(y) = \sum_{k=0}^{n}(-1)^k\frac{(n+|m|)!}{(n-k)!\ (|m|+k)!\ k!}y^k. \tag{A.154}$$

Two recurrence relations are often used to generate the polynomials in a successive way. They are given as

$$\sum_{i=0}^{n} L_i^{|m|}(y) = L_n^{|m|+1}(y), \tag{A.155}$$

and

$$L_n^{|m|}(y) = L_n^{|m|+1}(y) - L_{n-1}^{|m|+1}(y). \tag{A.156}$$

A solution for the eigenvector are now obtained. If we now substitute back and do some simple algebra we get the unnormalized eigenvector corresponding to Eq. (A.126)

$$\psi(r) \propto \beta^{(|m|+1)/2} r^{|m|} e^{-\beta r^2/2} L_n^{|m|}(\beta r^2). \tag{A.157}$$

To find the eigenvalues, we start with

$$n = \frac{1}{2}\left(\frac{\epsilon}{2\beta} - m - 1\right). \tag{A.158}$$

Remember that we need to use absolute values of m to rule out divergent solutions. Substitute Eq. (A.158) back into Eq. (A.127) we get the eigenvalues

$$E = (2n + |m| + 1)\hbar\omega + m\hbar\omega_B. \tag{A.159}$$

What is left in this section is to normalize the eigenvectors. Due to finite probability the normalization condition is

$$C^2\int_\Omega \Psi_{N'}^\dagger \Psi_N d\Omega = \delta_{N'N}. \tag{A.160}$$

Where Ω is our model space and Ψ are the eigenvectors that need to be normalized. C gives us the normalization factor. We need to normalize the radial part $\psi(r)$. When we normally transform an area integral with differentials $dxdy$ into cylindrical polarcoordinates we get $dxdy = rdrd\theta$. See Appendix A.3. Calculation will not be shown in detail, since they have very limited illustrative purpose. For the radial part Eq. (A.160) is given as

$$C_r^2\int_0^\infty \beta^{|m|+1} r^{2|m|} e^{-\beta r^2} L_n^{|m|}(\beta r^2) L_{n'}^{|m|}(\beta r^2) r dr = \delta_{n'n}. \tag{A.161}$$

Substitute $x = \beta r^2$ and simplify

$$\frac{C_r^2}{2}\int_0^\infty x^m e^{-x} L_n^{|m|}(x) L_{n'}^{|m|}(x) dx = \delta_{n'n}. \tag{A.162}$$

We can now use the property that the associated Laguerre polynomials are orthogonal over $[0, \infty)$ (FINN REF) with respect to the weighting function $x^{|q|}e^{-x}$, that is

$$\int_0^\infty x^{|q|} e^{-x} L_r^{|q|}(x) L_s^{|q|}(x) = \frac{(r+|q|)!}{r!}\delta_{sr} \tag{A.163}$$

Now, this is very similar to Eq. (A.162) and we see that we get the normalization factor for the mass-center part

$$C_r = \sqrt{\frac{2n!}{(n+|m|)!}} \tag{A.164}$$

Including the normalization factors we get the total normalized eigenvector for the two dimensional harmonic oscillator.

$$\psi_{nm}(r) = \sqrt{\frac{2n!}{(n+|m|)!}}\beta^{(|m|+1)/2} r^{|m|} e^{-\beta r^2/2} L_n^{|m|}(\beta r^2). \tag{A.165}$$

If we now make use of Eq. (A.154) and the substitution $\rho^2 = \beta r^2$, the eigenvector above can be written as

$$\psi_{nm}(\rho) = \sqrt{\beta}\rho^{|m|} e^{-\rho^2/2} \sum_{k=0}^{n} a_{nmk}\rho^{2k}, \tag{A.166}$$

where

$$a_{nmk} = (-1)^k \frac{\sqrt{2n!\ (n+|m|)!}}{(n-k)!\ (|m|+k)!\ k!}. \tag{A.167}$$

A.6.2 Three dimension

In three dimension the Schrödinger equation has the following form

$$-\frac{\hbar^2}{2m^*}\left\{\frac{\partial^2}{\partial r^2} + \frac{2}{r}\frac{\partial}{\partial r} - \frac{l(l+1)}{r^2} - \frac{emB}{\hbar c}\right\}\psi(r) + \frac{1}{2}m^*\omega^2 r^2\psi(r) = E\psi(r). \tag{A.168}$$

Again, define

$$\epsilon = \frac{2m^*E}{\hbar^2} - \frac{emB}{\hbar c}, \tag{A.169}$$

and substitute

$$\psi(r) = \frac{1}{r}u(r), \tag{A.170}$$

into Eq. (A.168) to get

$$-\frac{\partial^2 u(r)}{\partial r^2} + \left(\frac{l(l+1)}{r^2} + \frac{m^* 2\omega^2 r^2}{\hbar^2}\right)u(r) = \epsilon u(r). \tag{A.171}$$

We need to make the equation dimensionless. Substituting $\rho = \sqrt{m^*\omega/\hbar}r = \sqrt{\beta}r$ into the equation above, and at the same time defining

$$\epsilon' = \frac{\epsilon}{\beta}, \tag{A.172}$$

results in the equation

$$-\frac{\partial^2 u'(\rho)}{\partial\rho^2} + \left(\frac{l(l+1)}{\rho^2} + \rho^2\right) u'(\rho) = \epsilon' u'(\rho). \tag{A.173}$$

Considering the limit $\rho \to \infty$ just like we did for the two dimensional case, we see that we can do the substitution

$$u'(\rho) = e^{-\rho^2/2} p(\rho). \tag{A.174}$$

This give rise to

$$-\frac{\partial^2 p(\rho)}{\partial\rho^2} + 2\rho\frac{\partial p(\rho)}{\partial\rho} + \left(\frac{l(l+1)}{\rho^2} + 1 - \epsilon'\right) p(\rho) = 0. \tag{A.175}$$

Just like we did for two dimensions we can represent $p(\rho)$ as a series. By using Eq. (A.141) and its derivatives in Eq. (A.142) and (A.143) with y replaced by ρ we get the equation

$$\sum_{n=0}^{\infty} \left[2\rho^2(n+\sigma) - (n+\sigma)(n+\sigma-1) + l(l+1) + \rho^2(1-\epsilon')\right] a_n \rho^n = 0. \tag{A.176}$$

First observe that for $\rho = 0$ we can get divergence for $n < 2$ unless $a_1 = 0$. As a consequence of this, all odd terms vanish. Using the same arguments as for two dimensions, we get the indicial equation

$$\sigma(\sigma-1) = l(l+1). \tag{A.177}$$

This equations has two solutions. The first, $\sigma = -l$ give a divergence for $\rho = 0$ and cannot be allowed. The last solution is valid in our case, since $\sigma = l+1$ does not give rise to any divergences. Substituting this value back into Eq. (A.176) and sorting terms we get

$$\sum_{n=0}^{\infty} \left[(2(n+l)+3-\epsilon')a_n - ((n+2l+3)(n+2))a_{n+2}\right] a_n \rho^n = 0 \tag{A.178}$$

For this equation to be satisfied we require that the coefficient of each power of ρ vanish separately. The recurrence relation are then

$$a_{n+2} = \frac{2(n+l)+3-\epsilon'}{(n+2l+3)(n+2)} a_n. \tag{A.179}$$

We need the series to terminate at $n = n'$. This is satisfied if

$$\epsilon' = 2(n'+l)+3. \tag{A.180}$$

Remember that for odd values of n, the series completely zeros. Only even values of n are relevant. Let us define $n = 2k$ and $n' = 2k'$, where $k, k' = 0, 1, 2....$ Using the relations in Eq. (A.169), (A.172), (1.18) and in addition redefine $k' = n$ we get the eigenvalues corresponding to Eq. (A.168)

$$E = \left(2n + l + \frac{3}{2}\right)\hbar\omega + m\hbar\omega_B. \tag{A.181}$$

Where $l = 0, 1, 2, ...$ and $m \leq l$. The recurrence relation becomes

$$a_{2k+2} = \frac{k - k'}{(k + l + 3/2)(k + 1)} a_{2k}. \tag{A.182}$$

Notice the similarities with Eq. (A.150). In fact we can make use of this. By writing the recurrence relation above for even values of the polynomial we get

$$a_{k+1} = \frac{k - k'}{(k + l + 3/2)(k + 1)} a_k, \tag{A.183}$$

which is exactly equal to Eq. (A.150) apart from one constant term. Since we used the substitution $x = r^2$ in the two dimensional case, the polynomials are also the same, apart from the constant term. The constant term can be shifted. By using all the same arguments as in Ap. A.6.1 with slight modification due to the extra dimension, we get the normalized eigenvector

$$\psi_{nl}(r) = \sqrt{\frac{2n!}{(n + l + 1/2)!}} \beta^{(l+3/2)/2} r^l e^{-\beta r^2/2} L_n^{l+1/2}(\beta r^2). \tag{A.184}$$

Where we have redefined $k' = n$. The Laguerre polynomials $L_n^{l+1/2}$ are discussed in the end of Ap. A.6.1. We may again rewrite the eigenfunction as a finite series using the substitution $\rho^2 = \beta r^2$ and Eq. (A.154). This would give

$$\psi_{nl}(r) = \beta^{3/4} \rho^l e^{-\rho^2/2} \sum_{k=0}^{n} a_{nlk} \rho^{2k}, \tag{A.185}$$

where

$$a_{nlk} = (-1)^k \frac{\sqrt{2n!\ (n + l + 1/2)!}}{(n - k)!\ (l + k + 1/2)!\ k!}. \tag{A.186}$$

A.7 Exact solution for the interacting part

We will in this section solve the two particle Coulomb interaction problem exact. This method are outlined in [21]. It is a very special and limited case, but it is nevertheless important. The Schrödinger equation in question is

$$H_r \Psi = E_r \Psi. \tag{A.187}$$

The Hamiltonian for the electron-electron interaction have the following form

$$H = -\frac{\hbar^2}{2\mu}\left(\frac{\partial^2}{\partial r^2} + \frac{1}{r}\frac{\partial}{\partial r} + \frac{1}{r^2}\frac{\partial^2}{\partial \theta^2} + i\frac{eB}{\hbar c}\frac{\partial}{\partial \theta}\right) + \left(\frac{1}{2}\mu\omega^2 r^2 + \frac{e^2}{8\pi\epsilon\epsilon_0 r}\right). \tag{A.188}$$

As in Section A.6.1 the eigenvectors are separable in r and θ.

$$\Psi(r,\theta) = e^{im\theta}\psi(r) \tag{A.189}$$

We can then put the Hamiltonian into Schrödinger equation, do the substitution and obtain the equation

$$-\frac{\hbar^2}{2\mu}\left(\frac{\partial^2}{\partial r^2}+\frac{1}{r}\frac{\partial}{\partial r}-\frac{m^2}{r^2}-\frac{emB}{\hbar c}\right)\psi(r)+\left(\frac{1}{2}\mu\omega^2 r^2+\frac{e^2}{8\pi\epsilon\epsilon_0 r}\right)\psi(r)=E_r\psi(r). \tag{A.190}$$

Which has similarities with the solution for the non-interacting case, however, the interacting term will yield significant complication in the solution process. First we include the constant term into the energy by defining

$$E_r' = \frac{2\mu E_r}{\hbar^2}-\frac{emB}{\hbar c}. \tag{A.191}$$

To get rid of the single derivative, substitute

$$\psi(r) = r^{-1/2}u(r), \tag{A.192}$$

into the equation. Sorting terms give

$$-\left(\frac{\partial^2}{\partial r^2}+\left(\frac{1}{4}-m^2\right)\frac{1}{r^2}\right)u(r)+\left(\frac{\mu^2\omega^2}{\hbar^2}r^2+\frac{\mu e^2}{4\pi\hbar^2\epsilon\epsilon_0 r}-E_r'\right)u(r)=0. \tag{A.193}$$

Again we introduce another substitution to make the coordinate dimensionless

$$\rho = \sqrt{\frac{\omega\mu}{\hbar}}r, \tag{A.194}$$

After doing this we have the equation

$$\left(\frac{\partial^2}{\partial\rho^2}+\left(\frac{1}{4}-m^2\right)\frac{1}{\rho^2}\right)u'(\rho)-\left(\rho^2+\frac{l_0}{a_0'\rho}-\epsilon_r\right)u'(\rho)=0, \tag{A.195}$$

where

$$l_0 = \sqrt{\frac{\hbar}{\mu\omega}}, \tag{A.196}$$

$$a_0' = \frac{4\pi\epsilon\epsilon_0\hbar^2}{e^2\mu}, \tag{A.197}$$

$$\epsilon_r = \frac{\hbar E_r'}{\mu\omega}. \tag{A.198}$$

The constant a_0' is known as the Bohr radius if we replace the reduced mass, by the true electron mass. We now consider the isolated case for $\rho \to \infty$. As ρ increase, the Coulomb repulsion decrease and when ρ is big enough we can disregard it. For the non-interacting case we saw that we then had a solution

$$u(\rho) \simeq e^{-\rho^2/2}, \tag{A.199}$$

when $\rho \to \infty$. Since the interacting case also exist when ρ approaches infinity we know that this is part of our solution and we can substitute

$$u(\rho) = e^{-\rho^2/2} p(\rho), \tag{A.200}$$

into Eq. (A.195) and get

$$\left(\frac{\partial^2}{\partial \rho^2} - 2\rho \frac{\partial}{\partial \rho} + \left(\frac{1}{4} - m^2 \right) \frac{1}{\rho^2} - \frac{l_o}{a_0' \rho} - 1 \right) p(\rho) + \epsilon_r p(\rho) = 0. \tag{A.201}$$

We now need to do a series expansion. Looking at the equation we see that we've a singularity at $\rho = 0$ and a irregular singularity at $\rho = \infty$. We can then use the Frobenius series as we did in the non-interacting case. Using the expansion

$$p(\rho) = \sum_{n=0}^{\infty} a_n \rho^{n+\sigma}, \tag{A.202}$$

with the derivatives

$$\frac{\partial p(\rho)}{\partial \rho} = \sum_{n=0}^{\infty} (n+\sigma) a_n \rho^{n+\sigma-1} \tag{A.203}$$

$$\frac{\partial^2 p(\rho)}{\partial \rho^2} = \sum_{n=0}^{\infty} (n+\sigma-1)(n+\sigma) a_n \rho^{n+\sigma-2}. \tag{A.204}$$

Now, put Eq. (A.202), (A.203) and (A.204) into Eq. (A.201), then sort terms to get

$$\sum_{n=0}^{\infty} \left\{ (n+\sigma-1)(n+\sigma) - 2(n+\sigma)\rho^2 + \left(\frac{1}{4} - m^2 \right) - \frac{l_0 \rho}{a_0'} - (1-\epsilon_r)\rho^2 \right\} a_n \rho^n = 0. \tag{A.205}$$

Again, this equation should be valid for all ρ. If we put $\rho = 0$ all terms with $n > 0$ disappears and we're left with the indicial equation

$$(\sigma - 1)\sigma + \left(\frac{1}{4} - m^2 \right) = 0. \tag{A.206}$$

Solving this equation gives two solutions

$$\sigma = \frac{1}{2} \pm m. \tag{A.207}$$

Since this is a physical system, we don't want divergent solutions. Looking at the first solution $\sigma = 1/2 - m$ we see that this gives divergence at $\rho = 0$ if $m > 0$. We can not allow this and the second solution is accepted as long as we only use positive values of m. The series expansion that will give a solution is

then

$$p(\rho) = \rho^{1/2+|m|} \sum_{n=0}^{\infty} a_n \rho^n \tag{A.208}$$

Looking at equation Eq. (A.205) we can derive the recurrence relation by doing variable a variable change and resorting term. This results in

$$\begin{aligned} \sum_{n=0}^{\infty} \quad & \Big\{ \quad \left((n+\sigma-1)(n+\sigma) + \left(\frac{1}{4} - m^2\right)\right) a_n \\ - \quad & (1 - \epsilon_r + 2(n+\sigma-2))\, a_{n-2} - \frac{l_0}{a_0'} a_{n-1} \Big\} \rho^n = 0. \end{aligned} \tag{A.209}$$

Again, this should be valid for all ρ giving rise to the recurrence relation

$$\begin{aligned} a_n \quad &= \quad \frac{1}{(n+\sigma-1)(n+\sigma) + \left(\frac{1}{4} - m^2\right)} \\ &\times \quad \left[(1 - \epsilon_r + 2(n+\sigma-2))a_{n-2} + \frac{l_0}{a_0'} a_{n-1}\right], \end{aligned} \tag{A.210}$$

insert $\sigma = 1/2 + |m|$ to get

$$\begin{aligned} a_n \quad &= \quad \frac{1}{\left(n+|m|-\frac{1}{2}\right)\left(n+|m|+\frac{1}{2}\right) + \left(\frac{1}{4} - m^2\right)} \\ &\times \quad \left[(1 - \epsilon_r + 2\left(n+|m|+\frac{1}{2}-2\right) a_{n-2} + \frac{l_0}{a_0'} a_{n-1}\right]. \end{aligned} \tag{A.211}$$

Some algebra yield

$$a_n = \frac{1}{n(n+2|m|)} \left[(2(n+|m|-1) - \epsilon_r)\, a_{n-2} + \frac{l_0}{a_0'} a_{n-1}\right]. \tag{A.212}$$

This equation is not valid for $n = 0$. We can now put the coefficients back into Eq. (A.202) and get a solution for $p(\rho)$

$$\begin{aligned} p(\rho) = \rho^{1/2+|m|} \quad & \Big[\quad 1 + \frac{l_0 \rho}{(1+2|m|)a_0'} + \frac{\rho^2}{2(2+2|m|)} \\ & \times \quad \left(2(1+|m|) - \epsilon_r + \frac{l_0^2}{(1+2|m|)a_0'^2}\right) + ...\Big] a_0 \end{aligned} \tag{A.213}$$

The constant a_0 need to be determined, but if we put $p(\rho)$ back into Eq. (A.201), we see that it does not matter what a_0 is as long as it is non-zero. Let us set $a_0 = 1$ for convenience. The series need to terminate at some n for normalizability to be fulfilled. Say that this n is just n. Then we demand that $a_n = 0$ and $a_{n+1} = 0$. Under these circumstances Eq. (A.212) give us a way to determine e_r in the following way. First

$$a_{n+1} \quad = \quad \frac{1}{(n+1)(n+1+2|m|)} \left[(2(n+|m|) - \epsilon_r)\, a_n + \frac{l_0}{a_0'} a_{n+1}\right] \tag{A.214}$$

observe that $a_n = 0$ and $a_{n+1} = 0$. Then solve for ϵ_r

$$\epsilon_r = 2(n + |m|). \tag{A.215}$$

We can simplify the expression for a_n by putting ϵ_r back into Eq. (A.212) and get

$$a_n = \frac{1}{n(n+2|m|)} \left[\frac{1}{k'} a_{n-1} - 2a_{n-2} \right]. \tag{A.216}$$

We defined ϵ_r as

$$\epsilon_r = \frac{\hbar}{\mu\omega} \left(\frac{2\mu E_r}{\hbar^2} - \frac{emB}{\hbar c} \right). \tag{A.217}$$

This and Eq. (A.215) give us the eigenvalues in Eq. (A.187)

$$E_r = (n + |m|)\hbar\omega + m\hbar\omega_B. \tag{A.218}$$

With ω and ω_B as previously defined. We now need to find the eigenvectors using back substitutions. The eigenvectors in this case cannot be simplified to known polynomials and we do need to generate each function with as many coefficient as n demands. By using Eq. (A.202) and substitute we get the eigenvector in Eq. (A.187) as follows

$$p(\rho)_{n,m} = \rho^{1/2+|m|} \sum_{k=0}^{n} a_k \rho^k, \tag{A.219}$$

first substitute $u(\rho) = e^{-\rho^2/2} p(r)$

$$u(\rho)_{n,m} = e^{-\rho^2/2} \rho^{1/2+|m|} \sum_{k=0}^{n} a_k \rho^k, \tag{A.220}$$

then $\rho = \sqrt{\omega\mu/\hbar}$

$$u(r)_{n,m} = e^{-\tilde{\omega}\mu r^2/2} (\tilde{\omega}\mu)^{(1/2+|m|)/2} r^{1/2+|m|} \sum_{k=0}^{n} a_k (\tilde{\omega}\mu)^{k/2} r^k, \tag{A.221}$$

and finally $\Psi(r) \propto e^{im\theta} r^{-1/2} u(r)$

$$\Psi(r,\phi)_{n,m} \propto e^{im\phi} e^{-\tilde{\omega}\mu r^2/2} (\tilde{\omega}\mu)^{(1/2+|m|)/2} r^{|m|} \sum_{k=0}^{n} a_k (\tilde{\omega}\mu)^{k/2} r^k \tag{A.222}$$

We can not normalize the r dependent part of this eigenvector analytically, since the polynomial becomes very complicated and cannot be generalized. The angle dependent function can easily be normalized as follows

$$\int_0^{2\pi} C_\theta^2 e^{-iM\theta} e^{iM\theta} d\theta = 1, \tag{A.223}$$

integrate and solve for C_θ gives

$$C_\theta = \frac{1}{\sqrt{2\pi}}. \tag{A.224}$$

For illustrative purpose, let us calculate the exact eigenvalue for $n = 2$. We have already defined $a_0 = 1$ and for $n = 2$, we also need a_1. Remember that we demanded that $a_2 = 0$ for normalizability to be fulfilled. From Eq. (A.216) we have

$$a_1 = \frac{l_0}{a_0'(1 + 2|m|)}, \tag{A.225}$$

using Eq. (A.216) and $a_2 = 0$ gives

$$\frac{l_0^2}{a_0'^2} = 2(1 + 2|m|). \tag{A.226}$$

This can be solved for ω, using Eq. (A.196) we get

$$\omega = \frac{\hbar}{2a_0'^2\mu(1 + 2|m|)}. \tag{A.227}$$

If we now use Eq. (A.218), substitute ω we get

$$E_r = (n + |m|)\frac{\hbar^2}{2a_0'^2\mu(1 + |m|)} + m\hbar\omega_B, \tag{A.228}$$

which is exact. At first this seem remarkable, but we must not forget that this solution only exist for specific ω values.

A.8 Expressions

This section lists expressions that are not derived. They are used in calculations and proper references are given.

A.8.1 Coefficient in matrix elements for the Coulomb interaction

For use in the series expansion of the energy matrix in combination with the Talmi integrals [20]. See [1, 2] for details.

$$\begin{aligned} B(n'm, nm, p) &= (-1)^{p-l}\frac{(2p+1)!}{2^{n'+n}p!} \\ &\times \sqrt{\frac{n'!n!(2n+2|m|+1)!(2n'+2|m|+1)!}{(n+|m|)!(n'+|m|)!}}\Lambda, \end{aligned} \tag{A.229}$$

where

$$\begin{aligned} \Lambda = \sum_{k=\nu}^{\xi} \Bigg[& \frac{(|m|+k)!(p-k)!}{k!(2k+2|m|+1)!(n-k)!(2p+1-2k)!} \\ & \times \frac{1}{(n'-p+|m|+k)!(p-|m|-k)!}\Bigg]. \end{aligned} \tag{A.230}$$

The summation limits are given by

$$\nu = \begin{cases} 0 & , \quad p-|m|-n' \leq 0 \\ p-|m|-n' & , \quad p-|m|-n' > 0 \end{cases} , \tag{A.231}$$

$$\xi = \begin{cases} p-|m| & , \quad p-|m| \leq n \\ n & , \quad p-|m| > n \end{cases} . \tag{A.232}$$

References

[1] T. A. Brody, G. Jacob, and M. Moshinsky. Matrix elements in nuclear shell theory. *Nucl. Phys.*, 17:16, 1960.

[2] T. A. Brody and M. Moshinsky. *Tables of transformation brackets.* Gordon and Breach, New York, 1967.

[3] M. Ciorga, A. S. Sachrajda, P. Hawrylak, C. Gould, P. Zawadzki, S. Jullian, Y. Feng, and Z. Wasilewski. Addition spectrum of a lateral dot from coulomb and spin-blockade spectroscopy. *Phys. Rev. B*, 61:16318, 2000.

[4] A. I. Ekimov, A. L. Efros, and A. A. Onushchenko. Quantum size effect in semiconductor microcrystals. *Solid State Commun.*, 56:921, 1985.

[5] M. M. FLER??!??!!? *The harmonic oscillator in modern physics: From atoms to quarks.* Gordon and Breach, New York, 1969.

[6] T. Fukui, S. Ando, and Y. Tokura. Gaas tetrahedral quantum dot structures fabricated using selective area metalorganic chemical vapor deposition. *Phys. Rev. Lett.*, 58:2018, 1991.

[7] G. H. Golub and C. F. V. Loan. *Matrix Computations.* Johns Hopkins, 1996.

[8] T. Heinzel. *Mesoscopic Electronics in Solid State Nanostructures.* Wiley-VCH, 2003.

[9] R. H. Landau and M. J. Páez. *Computational Physics.* John Wiley & Sons, New York, 1997.

[10] J. A. Lebens, C. S. Tsai, and K. J. Vahala. Applications of selective epitaxy to fabrication of nanometer scale wire and dot structures. *Appl. Phys. Lett.*, 56:2642, 1990.

[11] J.-Y. Marzin, J.-M. Gérard, A. Izraël, D. Barrier, and G. Bastard. Photoluminescence of singel inas quantum dots obtained by self-organized growth on gaas. *Phys. Rev. Lett.*, 73:716, 1994.

[12] P. Mohr and B. Taylor. *The 2002 CODATA Recommended Values of the Fundamental Physical Constants (Web Version 4.2). This database was developed by J. Baker, M. Douma, and S. Kotochigova. Available: http://physics.nist.gov/constants [2006, March 29].* National Institute of Standards and Technology, Gaithersburg, 2004.

[13] M. Moshinsky. Transformation brackets for harmonic oscillator function. *Nucl. Phys.*, 13:104, 1959.

[14] W. H. Press, S. A. Teukolsky, W. T. Vetterling, and B. P. Flannery. *Numerical Recipes in C.* Cambridge, 2002.

[15] M. A. Ratner. *Molecular Electronics.* Blackwell, 1997.

[16] S. Raymond, S. Fafad, P. J. Poole, A. Wójs, P. Hawrylak, S. Charbon-Neau, D. Leonard, R. Leon, P. M. Petroff, and J. L. Merz. State filling and time-resolved photoluminescence of excited states in $In_{1-x}Ga_xAs/GaAs$ self-assembled quantum dots. *Phys. Rev. B*, 54:11548, 1996.

[17] M. Reed, R. T. Bate, K. Brandshaw, W. M. Duncan, W. M. Frensley, J. W. Lee, and H. D. Smith. Spatial quantization in gaas-algaas multiple quantum dots. *J. Vacuum Sci. Technol. B*, 4:358, 1986.

[18] K. F. Riley, M. P. Hobson, and S. J. Bence. *Mathematical Methods. For physics and engineering.* Cambridge, 2003.

[19] R. Shankar. *Principles of Quantum Mechanics.* Kluwer Academic/Plenum Publishers, 1994.

[20] I. Talmi. *Helv. Phys. Acta*, 25:185, 1952.

[21] M. Taut. Two electrons in a homogeneous magnetic field: particular analytical solutions. *J. Phys. A:Math. Gen.*, 27:1045, 1994.